

Study of Wire Fabrication of Aluminum Treated with Diboride Particles

By

DAVID JAVIER FLORIÁN ALGARÍN

A thesis submitted in partial fulfillment of the requirements for the degree of

MASTER OF SCIENCE

In

MECHANICAL ENGINEERING

UNIVERSITY OF PUERTO RICO

MAYAGÜEZ CAMPUS

2014

Approved by:

O. Marcelo Suárez, PhD
President, Graduate Committee

Date

Pedro Quintero, PhD
Member, Graduate Committee

Date

Ricky Valentín, PhD
Member, Graduate Committee

Date

Ricky Valentín, PhD
Chairperson of the Department

Date

Samuel Hernández, PhD
Representative of Graduate Studies

Date

Abstract

The present thesis focuses on the fabrication of aluminum wires by adding XB_2 nanoparticles into an aluminum matrix, where X is a transition metal: Nb, Mg and Zr. The incorporation of aluminum in the XB_2 particles is normally a complex process due to lack of enough affinity between the components. Liquid aluminum has a high surface tension, combined with the unavoidable oxide layer that is formed externally on the diboride prevents proper contact between the particle and liquid aluminum at the fabrication temperatures. An alternative process is then needed for proper inoculation of Al with the diborides.

Diboride nanoparticles were obtained by fragmentation in a high energy ball mill and then mechanically alloyed with pure aluminum powder to form nanocomposite pellets. High energy ball milling was selected as the key process to achieve appropriate mixing and homogenization between components.

The XB_2/Al pellets were then sintered in a reduced vacuum atmosphere in order to increase the homogenization of the pellets and enhance the strength of diboride/aluminum interface.

The pellets of XB_2/Al were added into the molten aluminum and mixed. The treated melt was then poured into a cylindrical mold to produce cylindrical ingots, which were

subsequently cold-rolled to obtain wires with 1 mm diameter with a cross area reduction of 91%.

The wire specimens were mechanically characterized and their electrical resistivity was measured and compared with pure aluminum. The results obtained in this thesis clearly demonstrated the feasibility of improving the mechanical properties of the material without significantly affecting its electrical resistivity of the wires.

Resumen

El presente estudio se centra en la fabricación de alambres de aluminio mediante la adición de XB_2 nano partículas en una matriz de aluminio, donde x puede ser un metal de transición, en este caso, Nb, Zr y Mg. La incorporación de aluminio es XB_2 es un proceso complejo, debido a la falta de afinidad entre los componentes. El aluminio tiene una alta tensión superficial, combinado con la capa de óxido que se forma en la superficie de este la cual evita que el diboruro entre en contacto con el aluminio líquido.

Las nanopartículas se obtuvieron por la fragmentación en un molino de bolas de alta energía. Luego estas son mezcladas con polvo de aluminio puro para que estas se adhieran mecánicamente para formar unos gránulos (Nano compuestos). La trituración con el molino de bolas de alta energía fue seleccionada como un proceso clave para obtener una mezcla y la homogeneización adecuada entre los componentes.

Los XB_2/Al gránulos fueron sinterizados en una atmósfera de vacío reducida. Con el fin de aumentar la homogeneización de los gránulos y se ha aumentado la interfaz de diboruro/aluminio.

Los pellets de XB_2/Al se agregaron en el aluminio fundido y se mezclan. A continuación, la masa fundida tratada se vierte en un molde cilíndrico para producir lingotes cilíndricos, que fueron luego laminadas en frío para obtener cables con 1 mm de diámetro con una reducción del área transversal del 91%.

Las muestras de alambre se caracteriza mecánicamente y su resistividad eléctrica se midió y comparó con el aluminio puro. Nuestros resultados demuestran la viabilidad de mejorar las propiedades mecánicas del material, sin afectar significativamente su resistividad eléctrica.

Acknowledgements

I'm sincerely grateful to the University of Puerto Rico at Mayaguez, especially Mechanical Engineering program to let me growth my professional development.

I am particularly grateful to the Nanotechnology Center (National Science Foundation grant HRD 0833112) for providing funding my graduate studies and the development of this thesis. The authors would also like to thank Dr. O. M. Suarez's research group for their support in the project.

Special thanks to Prof. Xiaochun Li, currently at the University of California-Los Angeles that provided the master alloy aluminum containing 2% wt alumina nanoparticles was.

The tensile test machine was acquired through a grant provided by the Solid Waste Management Authority of Puerto Rico.

At last, but the most important I would like to thank my family and my wife Melina, for their unconditional support, inspiration and love.

Table of Contents

Abstract.....	ii
Resumen.....	iv
Acknowledgements	vi
Table of Contents.....	vii
List of Figures.....	ix
List of Tables.....	xii
Acronyms Used in the Research.....	xiii
1. Introduction.....	1
1.1 Literature Review.....	3
1.2 Research Objectives.....	8
1.3 Outline of the Research	9
2. Theoretical Background.....	10
2.1 Mechanical Alloying (MA) by Ball Milling	10
2.2 Composite.....	17
3. Experimental Procedure of Wire of Aluminum Treated with NbB ₂ and ZrB ₂ Nanoparticles.....	19
3.1 Results.....	23

4. Experimental Procedure of Wire of Aluminum Treated with MgB ₂ Nanoparticles	33
4.1 Results.....	34
5. Discussion	41
6. Conclusions.....	48
7. References.....	49
APPENDICES.....	54
APPENDIX A.	54
A.1 Experimental Procedure of Aluminum Wire Treated with Alumina Nanoparticles.	54
A.2. Results	55
A.4 Conclusions.....	67
APPENDIX B. Vario-Planetary Ball Milling Pulverisette 4 Fritsch™.....	68
B.1 Run setting for 10hr, 1600 rpm.....	68
B.1 Run setting for 1hr, 1000 rpm.....	69

List of Figures

Figure 1. Grinding medium.....	13
Figure 2 8000M Mixer/Mill.....	14
Figure 3 Planetary ball mill or Pulverisette.....	15
Figure 4 Attritor Mills [15].....	16
Figure 5 Manufacturing process of the wires.....	22
Figure 6 XRD pattern of ZrB ₂ specimen after 10 h of milling.....	23
Figure 7 Average computed NbB ₂ and ZrB ₂ particle size as a function of milling time. .	24
Figure 8 Secondary electron image of NbB ₂ particles: (A) As-received NbB ₂ (without ball milling); and (B) clusters of NbB ₂ particles after 10 milling hours.....	25
Figure 9 XRD pattern of ZrB ₂ /Al composite pellet after sintering.....	26
Figure 10 XRD pattern of NbB ₂ /Al composite pellet after sintering.....	27
Figure 11 Optical micrographs of the composite pellets: (A) NbB ₂ /Al pellet at low magnification; (B) NbB ₂ /Al pellet at higher magnification; (C) ZrB ₂ /Al pellet at low magnification; and (D) ZrB ₂ /Al pellet at higher magnification.....	27
Figure 12 Microstructures of the wires at different stages of the manufacturing process. (A) Aluminum ingot treated with 1 wt.% of NbB ₂ particles, (B) Aluminum wire containing 1 wt.% of NbB ₂ after cold rolling, (C) Aluminum with 1 wt.% NbB ₂ after (D) one can observe the grains of the final wire produced.....	29
Figure 13 Effect of levels of NbB ₂ and temperature in the electrical conductivity of aluminum wires (measured as percent of IACS).....	30

Figure 14 Effect of the ZrB_2 nanoparticles amount and temperature in the electrical conductivity of aluminum wires (measured as percent of IACS).	31
Figure 15 Measured tensile strength of aluminum wire samples.....	32
Figure 16 XRD pattern of MgB_2 specimen after 0 to 5 milling hours.....	34
Figure 17 Computed mean MgB_2 particle size as a function of milling time	35
Figure 18 Secondary electron image of MgB_2 particles: (A) As-received MgB_2 , i.e. without ball milling; and (B) clusters of MgB_2 particles after 5 milling hours.	36
Figure 19 XRD pattern of MgB_2/Al composite pellet after sintering.	37
Figure 20 Optical micrographs of the nanocomposite pellets: (A) Al/MgB_2 pellet at low magnification; (B) Al/MgB_2 pellet at higher magnification.	38
Figure 21 Effect of the MgB_2 nanoparticles and temperature on the electrical conductivity of aluminum wires (measured as percent of IACS).	39
Figure 22 Measured ultimate tensile strength of aluminum wire samples	40
Figure 23 Bending (looping) test of aluminum wires treated with different weight percentage of Al_2O_3 nanoparticles: (A) 0.25(B) 0.5(C) 0.75(D) 1.0.	56
Figure 24 Measured density of aluminum wire samples as a function of the amount of alumina added.....	57
Figure 25 Effect of the amount of alumina nanoparticles added and temperature on the electrical conductivity of aluminum wires (measured as percent of IACS).	58
Figure 26 Average ultimate tensile strength of aluminum wire samples as a function of alumina added.....	59

Figure 27. SEM images of tensile fracture surfaces of the aluminum wires treated with different weight percentage of Al_2O_3 nanoparticles: (A) 0.25 wt.%; (B) 0.5 wt.%; (C) 0.75 wt.%; and (D) 1.0 wt.%..... 60

Figure 28 Percent of brittle fracture area of aluminum wire samples treated with alumina nanoparticles..... 61

List of Tables

Table 1 ANOVA of the model electrical conductivity of the wires	43
Table 2 ANOVA of the model ultimate tensile strength	45
Table 3 ANOVA of the model in Equation 7	62
Table 4 ANOVA of the model in Equation 8	63
Table 5 Electrical conductivity analysis using the mixture rule	65
Table 6 Ultimate tensile strength analysis using the mixture rule	66

Acronyms Used in the Research

Some terms have been coined to explain process in the present research. The following list explains the expansions of some of the most commonly used acronyms:

Aluminum Matrix Composites	AMC
Extra High Conductivity	EHC
Deep Wire Drawing	DWD
High Conductivity	HC
International Annealed Copper Standard	IACS
Mechanical Alloying	MA
Matrix Composites	MC
Melt Extraction Technology	MET
Mechanical Milling	MM
Metal Matrix Composites	MMC
Process Control Agent	PCA
Scanning Electron Microscope	SEM
Standard Error	SE
X-ray Diffraction	XRD

1. Introduction

Naturally copper is one of the most common metallic materials used for electric wire applications [1]. Unfortunately, this metal presents the two main detrimental problems that can be found in transmission lines: corrosion susceptibility and mechanical damage by wind-induced movement due to the metal high ductility [2].

In aerospace applications, mechanical and electrical efficiencies are always pursued without adding weight to the aircraft [3]. According to Tyco Electronics Company, a 747 aircraft uses approximately 140 miles of wire weighing about 1,750 Kg.

For those reasons, light metal research and development are permanent endeavors. In particular, aluminum is one of the most commonly used light metals for this type of applications because of its low density and high electrical conductivity [4]. In effect, it ranks fourth among metals with the highest electrical conductivity whereas copper ranks second. Aluminum density is 2.70 g/cm^3 , while copper is 8.94 g/cm^3 .

Typically, to reduce the weight of the wires involves a high strength core material surrounded by a high conductivity metal. In that respect, the most common composite conductor type is an aluminum conductor reinforced with steel, which has been in use for more than 80 years [2]. In the last 15-20 years, aluminum alloys for electrical wires

have become more popular [2]. Research and fabrication of copper-clad aluminum wire had been in development without converting results due to the low mechanical strength of the aluminum wire [5].

In the aerospace industry, one way to increase the efficiency of energy consumption is to lower the weight of the aircraft by substituting the material used for the electrical wiring. Since aluminum is three times less dense than copper, it would be a better alternative for aircraft; however, aluminum has some properties that are not appealing: low Young's modulus (compared to that of copper), high ductility and susceptibility to plastic deformations during long exposures to a constant forces and high temperatures (low creep resistance) [6].

For this reason, the present project focused on the reinforcement of aluminum wires by adding nanoparticles of NbB_2 , MgB_2 , and ZrB_2 in order to strengthen the metal without significantly affecting its electric resistivity and density. The wires are also expected to be used as soldering material for space welding of aluminum parts where the diboride particles can provide additional strength to the weld.

1.1 Literature Review

As mentioned, copper is one of the most popular metallic materials used for electric wire applications [1]. On the other hand, the direct industrial importance of conductivity in aluminum alloys is best emphasized by the extensive use of aluminum alloys as electrical conductors in power lines. Production of high conductivity and extra high conductivity wires is important in the bare and insulated conductor industry because of the saving in energy cost during the entire service life [2].

1.1.1. Deep Wire Drawing (DWD)

- Hanazaki et al. studied how the process of continuous wire drawing would affect the microstructure, mechanical, and electrical properties of wires [1]. The material used for this process was pure copper wire with an initial diameter of 7.5 mm. In their wire drawing process, copper wires underwent 21 drawing steps to reduce the wire diameter to 0.236 mm, achieving a total reduction of area of 99.90%. The authors observed that the electrical conductivity of the copper wires not affected by the continuous wire drawing process and that the tensile strength increased as reduction of area increased [1].

1.1.2. Draw-Bending Process

- Draw-bending is a process where the wire is bent to a 90° angle after cold rolling, annealing, and 23 passes through wire drawing [7], [8]. Tokutomi et al. used a die designed to decrease the drawing tension and to prevent the formation of any irregular cross-sectional shape by the rotation of the shaft [7]. They concluded that the changes in hardness and mechanical properties were closely related to the metallographic structure.

1.1.3. Melt Extraction Technology (MET)

- Wang et al. aimed at establishing an optimum process for fabricating fine Cu-based amorphous wires with circular cross section [9]. They proposed a concept called melt extraction using a high-speed wheel with a sharp edge in contact with the molten alloy surface, which was then rapidly; The thus, the molten layer turned into solid wires [9]. After finding the optimum parameters to fabricate fine and uniform circular wires, they conducted several tensile strength tests on their specimen and measured relatively higher tensile strengths in the fabricated wires.

1.1.4. Clad and Chip

- This work by Tang et al. focused on the fabrication of wires/rods via friction extrusion process [10]. The materials selected were aluminum alloys AA2050 and AA2195 chips. By using the friction extrusion process to manufacture wire and rods, grains became finer in the processed zone due to high temperatures. Through a thoroughly discussed procedure, they discovered that the hardness of the wires were relatively homogeneous and that the wires demonstrated good bend ductility [10].

1.1.5. Cold Drawing and Aging

- The first objective of T. Sasaki is section was to analyze an alternative process to form ultra-fine grains at the Cu/Al interface to reduce or even eliminate the continuous intermetallic layers and/or filamentary microstructure that can form at the interface [5]. The authors used copper-clad aluminum with drawing and heat treatment to produce the wire with ultra-fine grains. They wrapped a copper strip of 0.5 mm of thickness around an aluminum rod of 20 mm of diameter. Then, by cold drawing, the diameter was reduced from 18 mm to 2 mm and the wire was heat treated at 315⁰C for 5 h. The final cold drawing reduced the diameter from 2 mm to 1 mm. The authors found that in the heat-treated wire, continuous intermetallic phases (Al₂Cu, AlCu, and Al₄Cu₉) formed at the Cu/Al interface [5].

1.1.6. Critical Assessment of the Surveyed Literature

DWD is an effective and inexpensive process used to decrease the diameter of the wire. Interestingly, this method also decreases the tensile strength of the material. In the MET procedure, an amorphous wire with circular cross section was fabricated through a rather complex methodology [10]. Yet, this process produces relatively homogeneous wires that exhibit good mechanical properties. For large-scale applications, it seems like a viable option but not necessarily for small-scale ones. The fabrication of wires via cold-working and aging is fairly easy to use and to reproduce. Although, because of the cost of the homogenization of the ingots at high temperatures for long time and the hot rolling of the ingots, this may not be the most economic fabrication method [11].

Although there are numerous publications about conductive wire fabrication, these are mostly based in two methods. In the first one, copper is deformed to obtain a thin grain microstructure that improves the mechanical behavior of the metal. In the second one, copper and aluminum alloys are combined to reduce wire density. However, the main problem in trying to improve the mechanical properties through severe plastic deformation is that the material loses its ductility. With respect to the copper aluminum alloy, the challenge turns to be how to control secondary phase formation during the process.

In order to overcome issues related to cost, high conductivity, and high strength, we developed a procedure of aluminum wire fabrication where molten aluminum is treated with diboride nanoparticles that guarantees the lack of formation of new or unexpected phases and avoids using severe plastic deformation for strengthening purposes. Also the present research implements a methodology to obtain diboride nanoparticles and mechanically alloy them to form diboride/aluminum nanocomposite pellets using a milling process.

1.2 Research Objectives

Due to the lack of proper wettability between liquid Al and solid XB_2 particles, the aim of the present research was to develop a process to effectively insert those nanoparticles into a matrix of aluminum upon melting before wire cold forming.

Primary Objective

To improve mechanical properties of aluminum wire adding nanoparticles without significantly affecting the wire electrical conductivity.

Specific Objectives

- Implementation of effective method to inoculate molten aluminum with NbB_2 , MgB_2 and ZrB_2 nanoparticles.
- Manufacture an XB_2/Al wires in the laboratory.
- Evaluate of electrical properties and mechanical properties of the treated Al wires.

1.3 Outline of the Research

Chapter 2 deals with the theory and practice of ball milling process, and a summary of prior studies on aluminum matrix composites. Chapter 3 presents the complete procedure, as designed and developed to achieve the synthesis of the XB_2/Al nanocomposite at each process steps, i.e. ball milling and sintering, with the final incorporation of the XB_2 particles in the aluminum matrix. This is followed by a discussion on the wires fabrication process and the specimens characterization. Chapter 4 presents the complete procedure used for the synthesis of the MgB_2/Al composite following a similar structure to the fabrication of wires treated with the other XB_2/Al nanocomposites. The discussion of the results is presented in Chapter 5 while the conclusions are shown in Chapter 6. Appendix A presents additional experimentation with $\text{Al}_2\text{O}_3/\text{Al}$ composites used in the fabrication of wires.

2. Theoretical Background

2.1 Mechanical Alloying (MA) by Ball Milling

2.1.1 General Description

When powders of uniform composition are milled in a high-energy ball mill and material transfer is not required for homogenization, the process is termed as mechanical milling (MM). When a mixture of two metals is processed and alloying occurs, this is normally referred to as mechanical alloying because material transfer is involved. However, if a pure metal or an intermetallic is processed only to reduce particle size, then this will be referred to as MM because material transfer is not involved [12].

2.1.2 Mechanical Milling

The process of mechanical alloying starts with the preparation of the powders, which are weighed in the desired proportion and placed in the ball mill along with the grinding medium. Sometimes a process control agent is added to minimize excessive cold welding to the milling container and/or the grinding medium [13].

To achieve adequate particle size and/or properties, the optimization of a number of variables involved during MA becomes critical. As this was the case in the present thesis; the following fabrication parameters are discussed below, as they can greatly affect the final product after ball milling:

- ***Milling container***

Hardened steel, tempered steel, stainless steel, and tungsten carbide are the most common types of materials used for the jars. The internal shape of the container is important so there are no dead zones, which are the regions where the powder gets accumulated without getting milled [13]. In our case, we used tungsten carbide to avoid erosion by the hard diborides.

- ***Milling atmosphere***

To avoid contamination and to minimize oxidation of the milled powder, mechanical alloying can be conducted under vacuum or under an inert atmosphere [13]. In the present study the atmosphere could not be controlled in the instrumentation used.

- ***Milling speed***

Milling intensity or milling energy are terms used to describe the velocity of the milling process. High working speeds generate excessive wear on the jars and the grinding medium, which can produce contamination of the materials. When working with high velocities, the balls can be pinned to the inner walls of the jar and do not fall down to exert any impact force on the powders [13].

- ***Grinding medium***

The grinding medium affects directly the efficiency of the alloying or milling. The impact force on the powder should be high enough to promote mixing and mechanical alloying, and is affected by the size, density and material of the balls [13]. Materials commonly used are hardened steel, hardened chromium steel, stainless steel, and WC-Co. Figure 1 shows the grinding medium and jar used in the present research.



Figure 1. Grinding medium

2.1.3 Types of Mills

Different types of high-energy milling equipment are used to produce mechanically alloyed or milled powders, as described in the following sections [13].

- ***Spex shaker mills***

In Figure 2, one can observe an example of SPEX mills. Here the milling process is performed as back-and-forth; the elliptical movement is combined with lateral motion of the ends. These two motions generate a force of the balls impact unusually large [13].

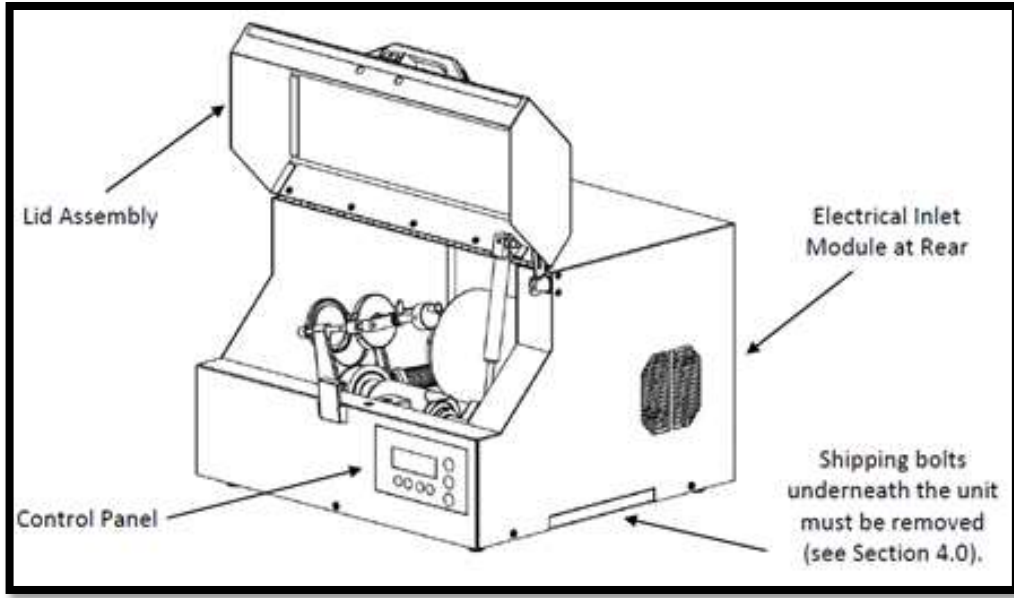


Figure 2 8000M Mixer/Mill [14]

- ***Planetary ball mills***

Another commonly utilized mill for conducting mechanical alloying experiments is the varioplanetary ball mill in which a few hundred grams of the powder can be milled at the same time. Figure 3 presents the Pulverisette 4 high energy ball mill, utilized in the present research.



Figure 3 Planetary ball mill or Pulverisette

In this milling unit, the containers and the supporting disk rotate in opposite directions producing centrifugal forces that act alternately in the same and opposite directions.

This causes two different effects:

- Friction effect: The grinding balls run down inside the jar walls.
- Impact effect: The sample material and balls lift off and travel freely through the inner container and collide with the opposite walls.

- **Attritor mills**

An attritor consists of a vertical drum containing a series of impellers rotating on its own axis to produce the movement of the grinding medium, as seen in Figure 4. The particles are subjected to various forces such as impact, rotation, and shear. Like the previous mills, this is not continuous, but one can control it to work as a continuous mill. As a consequence, this process is best suited for the continuous production of large quantities of material [13]

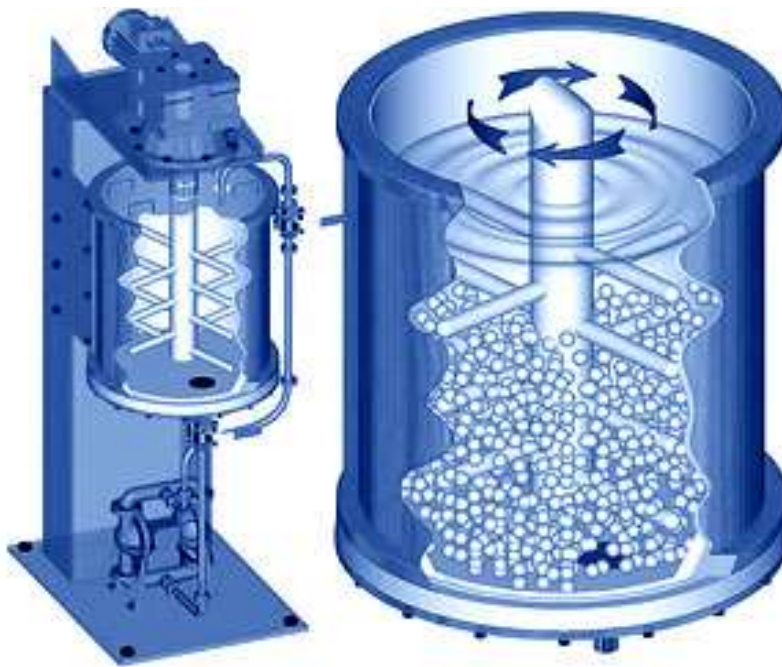


Figure 4 Attritor Mills [15]

2.2 Composite

2.2.1 Composite Materials

Composite materials are extending the horizons of engineering since these synthesized materials open the door to appealing solutions. In a composite, dissimilar materials are combined in such a way as to enable us to make better use of their individual and combined virtues while minimizing somehow the effects of their deficiencies [16].

2.2.2 Metal-Matrix Composites (MMC)

In these materials the common reinforcement of the metals are ceramic particles or fibers. The resulting materials possesses improved mechanical properties with the possibility of operating at higher temperatures [16].

Although multiple manufacturing methods have been used in a laboratory or industrial scale, there is still much work to do about the production processes for MMC [16]. Some of the most used techniques are:

- Unidirectional solidification of eutectics or other constitutionally-appropriate alloys.
- Liquid-phase infiltration during hot pressing of powder compacts containing whiskers or fiber bundles.
- Hot pressing of compacts consisting of matrix alloy sheets wrapped or interleaved with arrays of reinforcing wires.
- Hot pressing or drawing of wires pre-coated with the matrix alloy.
- Co-extrusion of prepared composite billets

3. Experimental Procedure of Wire of Aluminum Treated with NbB₂ and ZrB₂ Nanoparticles.

The present chapter describes the novel processing route of aluminum wires, which includes the incorporation of nanoparticles of NbB₂ and ZrB₂. This inoculation process of liquid aluminum cannot be achieved by the simple addition of the nanoparticles because of the lack of wettability between both phases, i.e. the diborides and the liquid metal. In a prior research, a varioplanetary high energy ball mill (discussed in a previous section) demonstrated to be effective in reducing diboride particle sizes by fragmentation [17]. In this research, the same equipment allowed fracturing as-received XB₂ particles to obtain nanosized diborides. The high energy ball mill operated at 1,600 rpm with tungsten carbide, grinding balls bearing 11.2 mm in diameter. All grinding parameters are shown in Appendix B. The diboride powders were then milled along with pure aluminum powder for one hour to form the diboride/Al pellets. These were then sintered at 260⁰C for half an hour in a reduced vacuum atmosphere (roughly 4 kPa), in order to increase the homogenization of the pellets and enhance the aluminum/diboride interface. Thus, the incorporation of aluminum into the nanocomposite pellet allowed better wetting by molten aluminum upon inoculation.

Commercially pure aluminum (99.0%) was then melted at 760⁰C, in a graphite crucible, inoculated with the sintered pellets, and mechanically stirred to improve the particle

distribution. The treated aluminum melt was poured into a cylindrical mold to produce 5 mm diameter ingots, which we then cold-rolled to make wires with 1.4 mm diameter with a cross area reduction of 92%. Full annealing at 400⁰C for 5 hours permitted to continue the cold rolling to reduce the wire diameter to 1 mm with a 96% final reduction in cross section area.

All samples were characterized by an x-ray (XRD) using a Siemens® D500 diffractometer, with Cu K α radiation ($\lambda = 0.154178$ nm). This procedure helped to: a) estimate both the nanoparticle size of NbB₂ and ZrB₂ using Scherrer's equation [18], and b) to analyze the XRD patterns of the composite pellets to determine whether unintended phases were formed upon milling. The microstructures of the specimens, i.e. as received powder, pellets, and wires (at different stages of the manufacturing process), were observed using a Nikon® Model Epiphot 200 optical microscope. Standard tensile tests at room temperature (25⁰C) were conducted in a low force universal testing machine Instron® model 5944.

A four-point probe technique was used to measure the wires electrical resistivity employing a convenient set up developed in a prior investigation [19]. This method records the voltage between two probing points while the different levels of currents are applied via two electrodes. Then, by measuring the sample geometry, one can compute the wire conductivity. The set up can also be immersed into ice-water and boiling water (100⁰C), to study how temperature affects the resistivity of the wires. In the present

research, the wires' electrical conductivity measurements were carried out at temperatures ranging from 0 to 100⁰C. Finally, electrical conductivity was expressed in terms of percent of the International Annealed Copper Standard (IACS) [20].

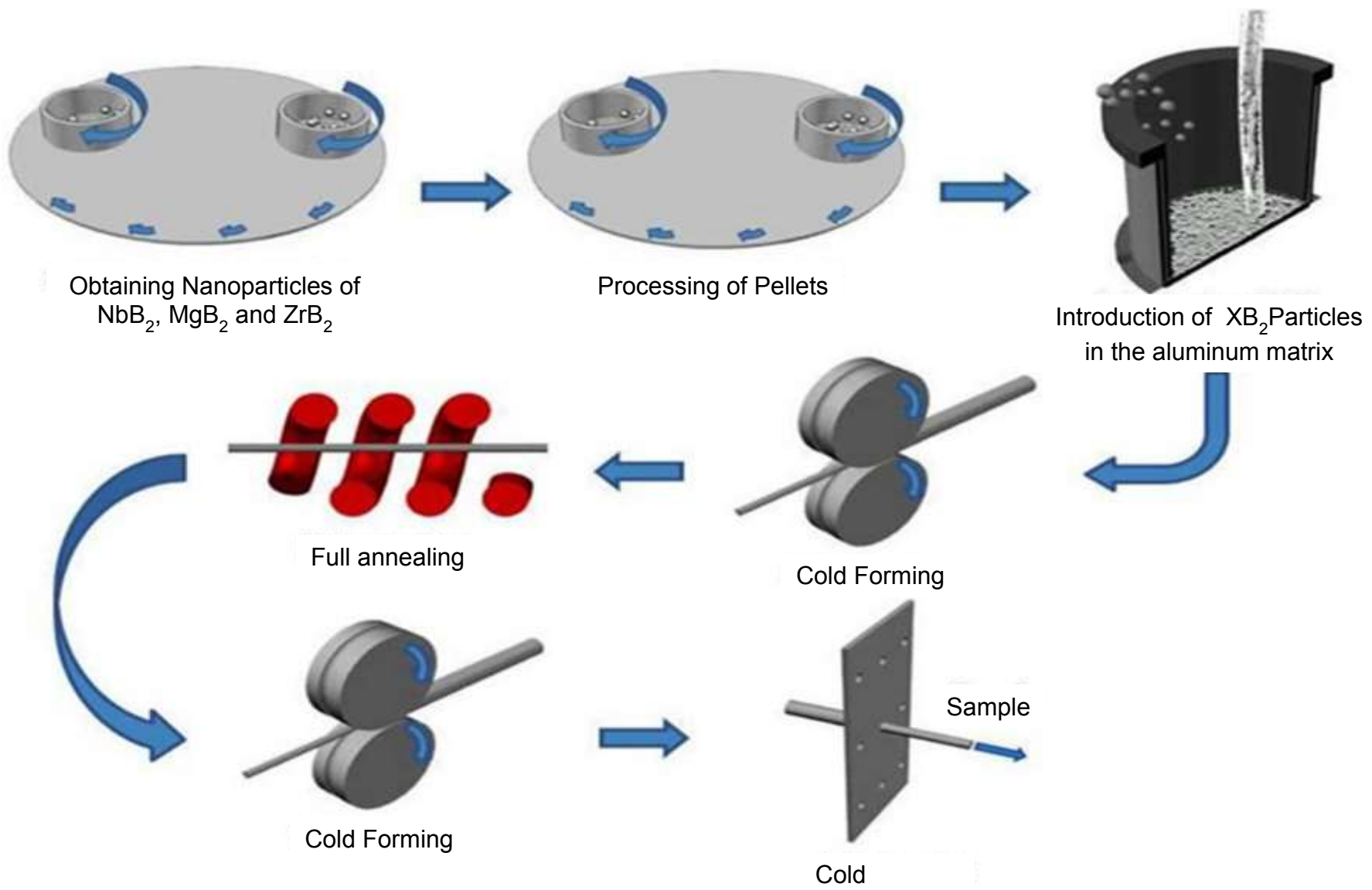


Figure 5 Manufacturing process of the wires

3.1 Results

3.1.1 NbB₂ and ZrB₂ Nanoparticles

To determine the most efficient milling procedure needed to produce the nanoparticles, different milling times were tested, ranging from 5 to 25 h for the NbB₂, while ZrB₂ powder was processed for 5 and 10 h. All milling parameters are presented in Appendix B. Figure 6 shows the x-ray diffraction pattern of the ZrB₂ specimen after 10 hours of milling, with the expected broad diffraction peaks.

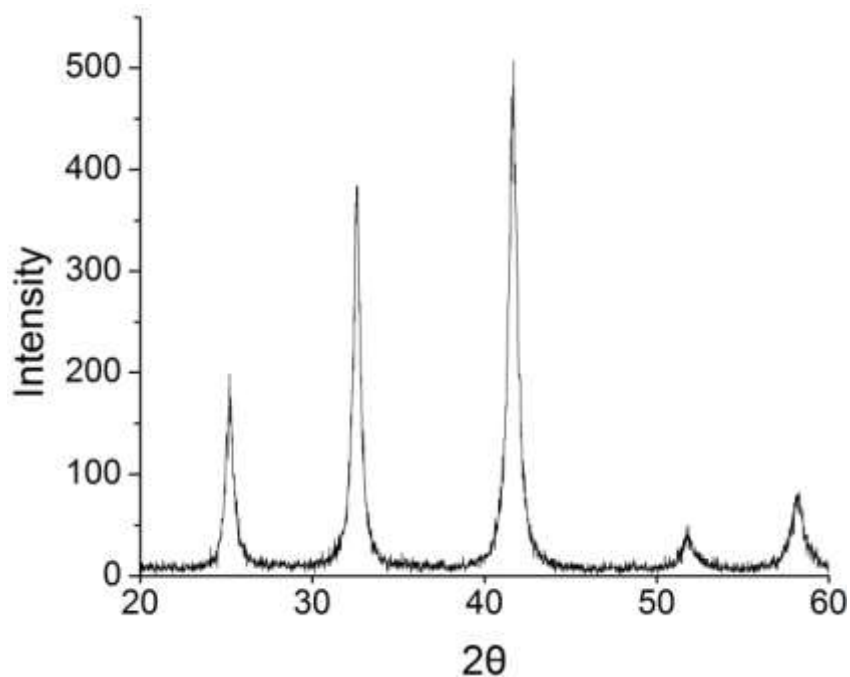


Figure 6 XRD pattern of ZrB₂ specimen after 10 h of milling.

As mentioned, the Scherrer equation permitted to estimate the average size of the ball milled diboride samples, based on the width of the largest XRD peak. Subsequent millings at different times demonstrated that after 10 h, the particle size remained almost constant, i.e. regardless of the milling time, as shown in Figure 7.

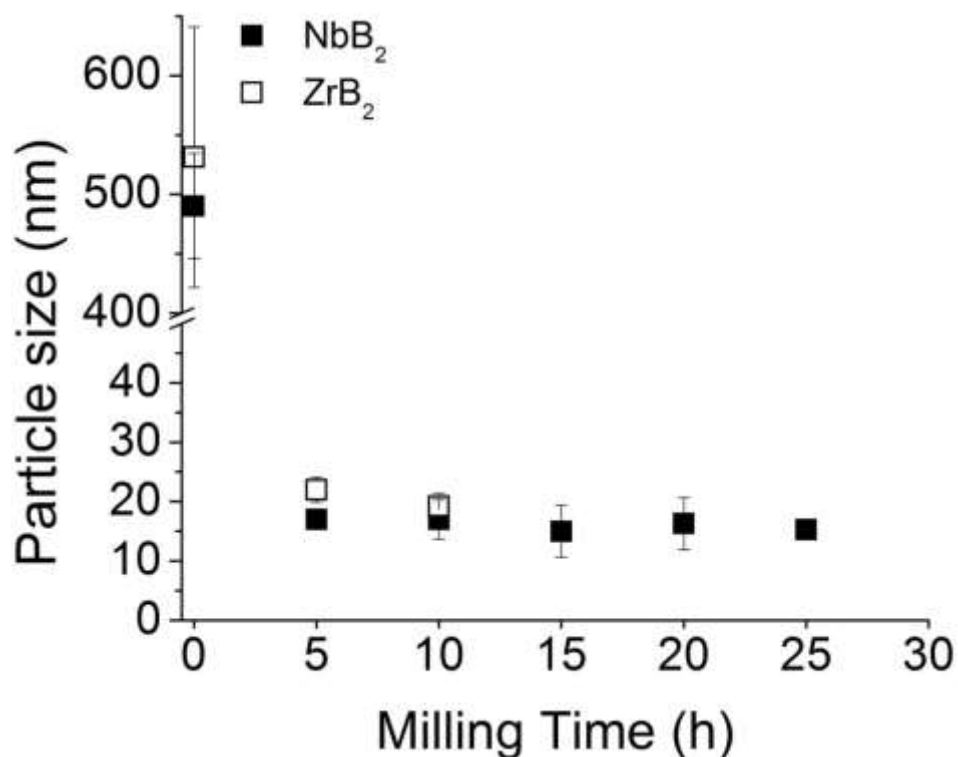


Figure 7 Average computed NbB₂ and ZrB₂ particle size as a function of milling time.

The scanning electron microscope (SEM) images in Figure 8 display NbB₂ particles before the ball milling process and after 10 h of milling. The reduction in particle size of the diboride is apparent. The NbB₂ particles obtained, which were milled for 10 h, had

an approximate size of 17 nm, which was deemed appropriate to proceed with the planned experiments.

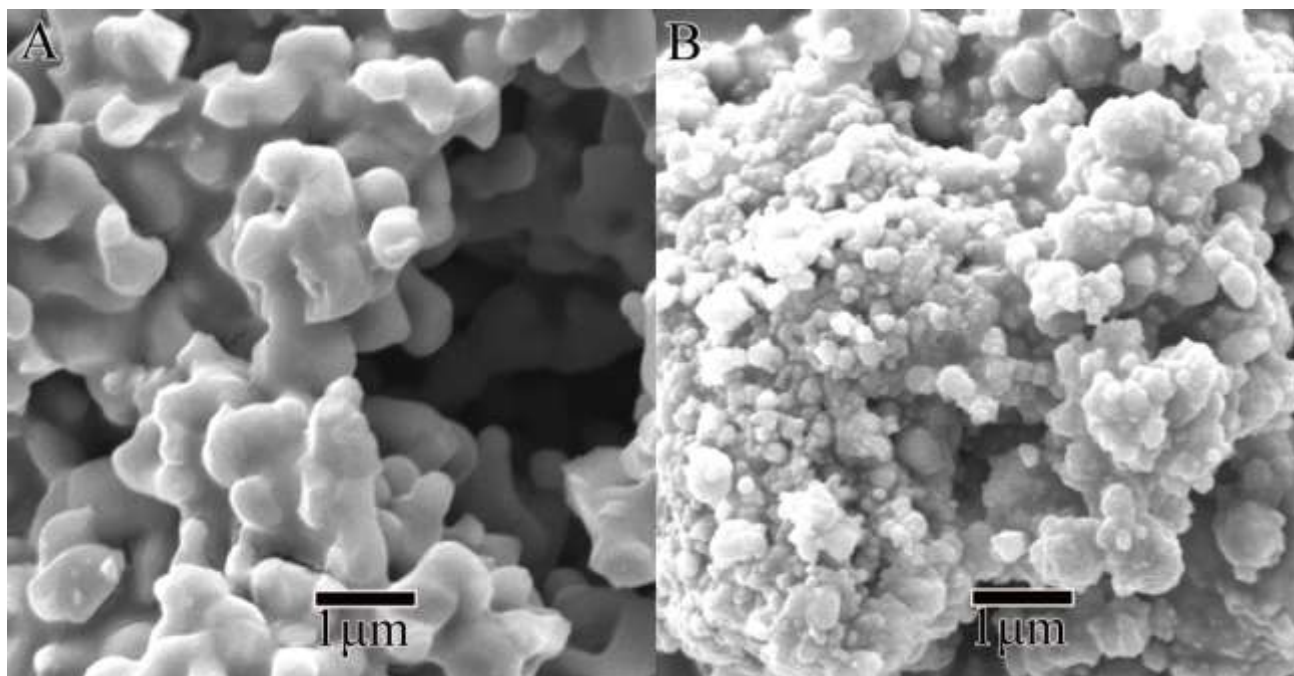


Figure 8 Secondary electron image of NbB₂ particles: (A) As-received NbB₂ (without ball milling); and (B) clusters of NbB₂ particles after 10 milling hours.

3.1.2 Nanocomposite Pellets

The nanosized diboride particles and 99.5% aluminum powder (average size of 44 μm) were mixed at 1000 rpm for one hour in the same ball milling unit to form the Al/diboride nanocomposite pellets. As mentioned, all pellets were then sintered at 260°C in a reduced pressure atmosphere. Figure 9 and Figure 10 respectively show the XRD patterns obtained from ZrB₂/Al and NbB₂/Al nanocomposite pellets. Apparently no

additional unintended phase (at least within detectable levels) was accidentally produced during the pellet fabrication.

Figure 11 shows representative microstructures of the sintered pellets. The images allowed corroborating that the diboride nanoparticles were well embedded in the Al matrix after milling.

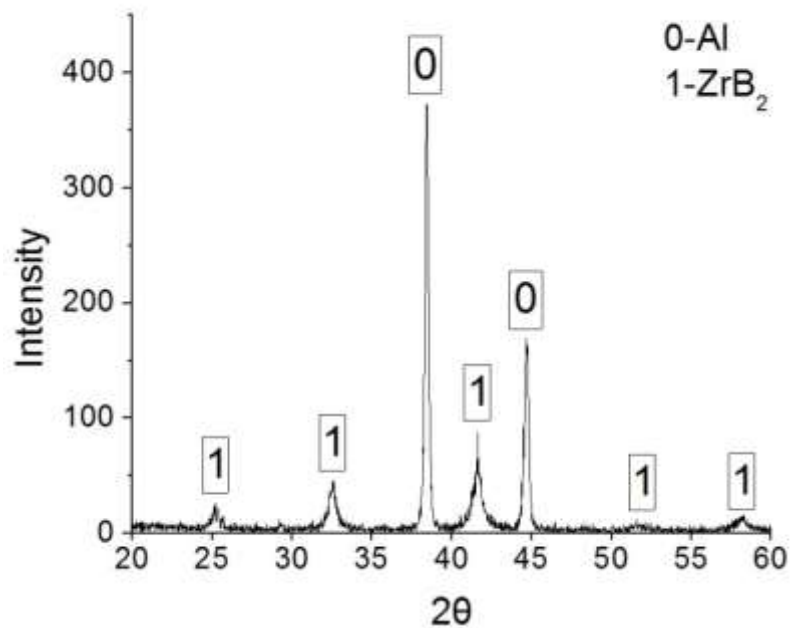


Figure 9 XRD pattern of ZrB₂/Al composite pellet after sintering.

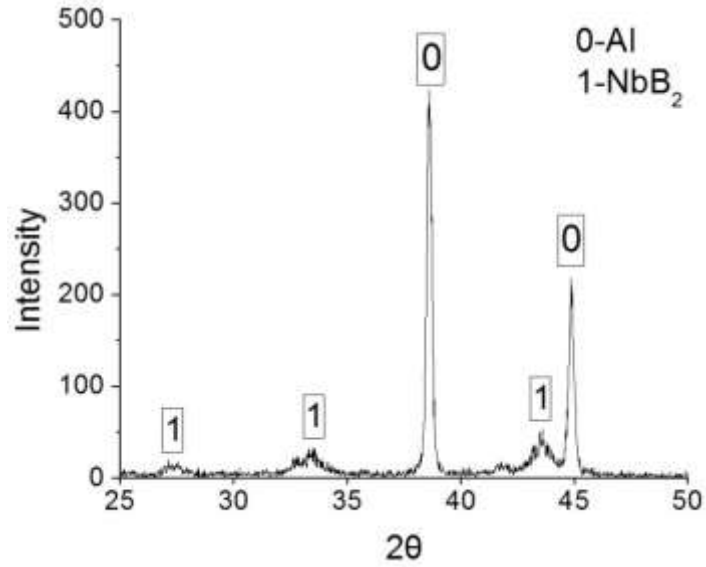


Figure 10 XRD pattern of NbB₂/Al composite pellet after sintering.

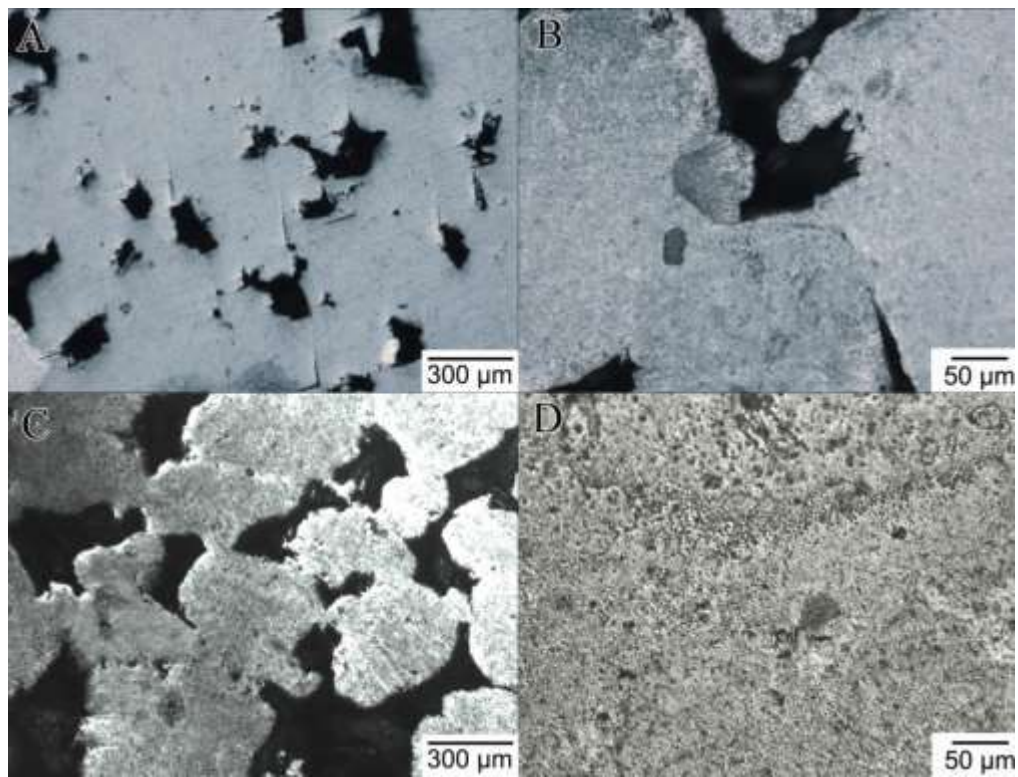


Figure 11 Optical micrographs of the composite pellets: (A) NbB₂/Al pellet at low magnification; (B) NbB₂/Al pellet at higher magnification; (C) ZrB₂/Al pellet at low magnification; and (D) ZrB₂/Al pellet at higher magnification.

3.1.3 Optical Micrographs of Treated Wires

Figures 11A through 11C show the microstructures of the aluminum wires at different stages of the manufacturing process, as observed in an optical microscope Figure 12. Figure 12 (A) shows the grain structure of as-cast ingot treated with 1 wt.% of NbB_2 , i.e. before cold working. In Figure 12 (B), one can observe how the grains in the Al-1wt% NbB_2 ingot are deformed with 92% cross-area reduction. In Figure 12 (C) the grain structure of the cold-formed specimen changes after full annealing is apparent. Full annealing at 400°C for 5 h permitted grain recrystallization, as seen in Figure 12 (C), In Figure 12 (D), one can observe the grains of the final wires produced.

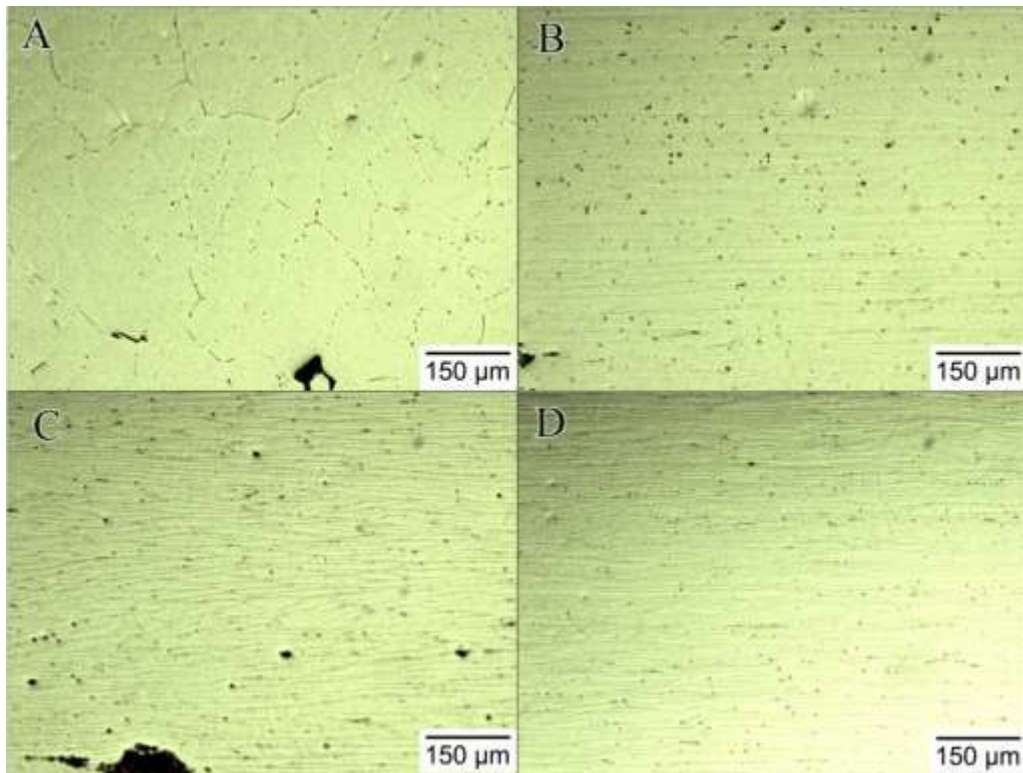


Figure 12 Microstructures of the wires at different stages of the manufacturing process. (A) Aluminum ingot treated with 1 wt.% of NbB₂ particles, (B) Aluminum wire containing 1 wt.% of NbB₂ after cold rolling, (C) Aluminum with 1 wt.% NbB₂ after cold rolling, (D) one can observe the grains of the final wire produced.

3.1.4 Electrical Conductivity

In the case of wires treated with NbB_2 , the conductivity decreased from 62.7% to 57.3 % IACS at 20°C, for NbB_2 concentrations from 0 to 3% percent, as observed in Figure 13. Figure 14 appears to demonstrate that for ZrB_2 , there is no significant change in the conductivity as the amount of nanoparticles increases. In both cases (NbB_2 and ZrB_2). Moreover and naturally, the electrical resistivity increased almost linearly with temperature.

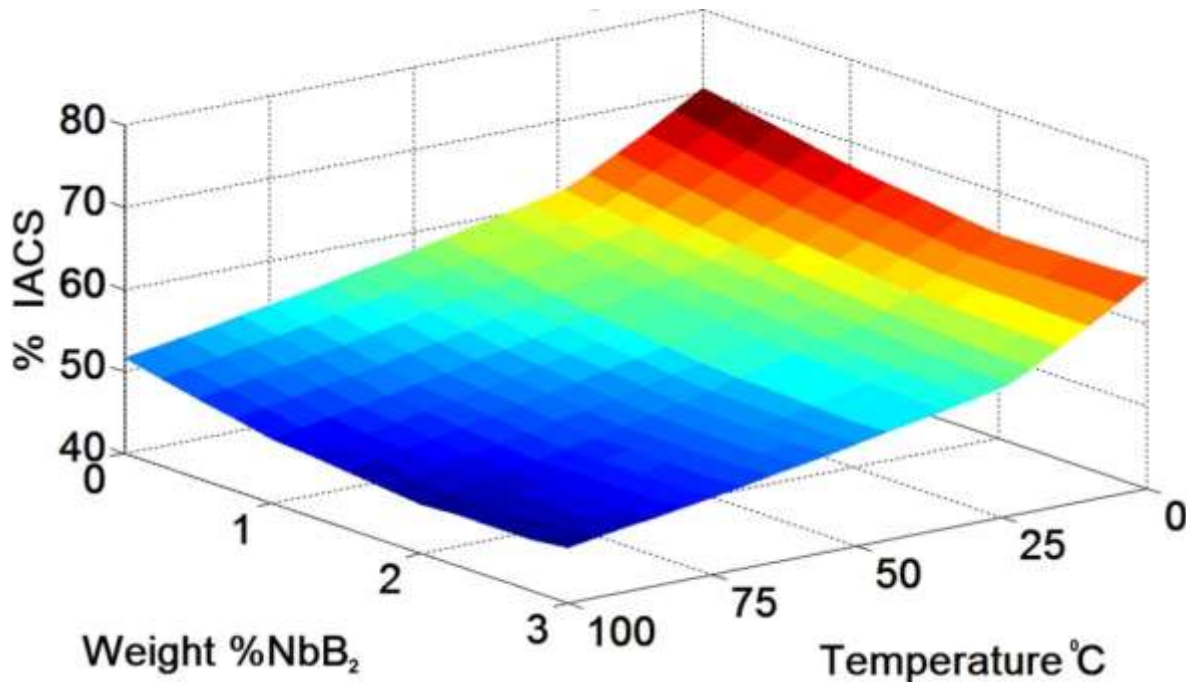


Figure 13 Effect of levels of NbB_2 and temperature in the electrical conductivity of aluminum wires (measured as percent of IACS).

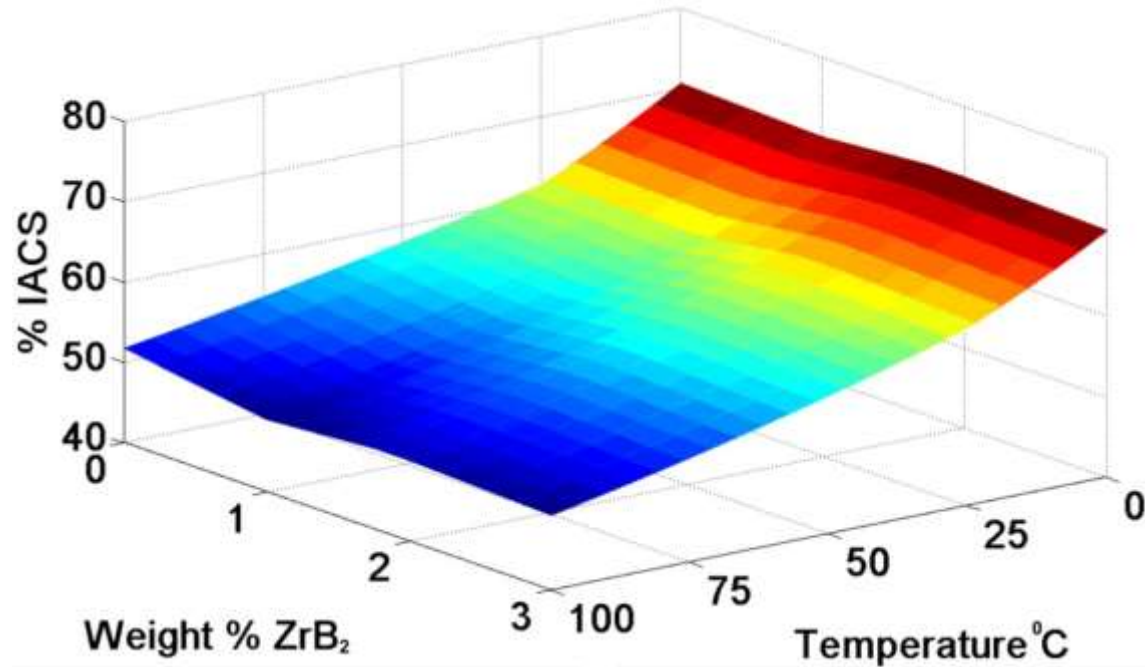


Figure 14 Effect of the ZrB₂ nanoparticles amount and temperature in the electrical conductivity of aluminum wires (measured as percent of IACS)

3.1.5 Tension Tests

As one can see in Figure 15, for both of the diborides studied, the minimum tensile strength increased as the amount of diboride nanoparticles added increases. The achieved tensile strengths of the aluminum wires became much higher than the strength normally reported for pure aluminum, i.e. 70MPa [21].

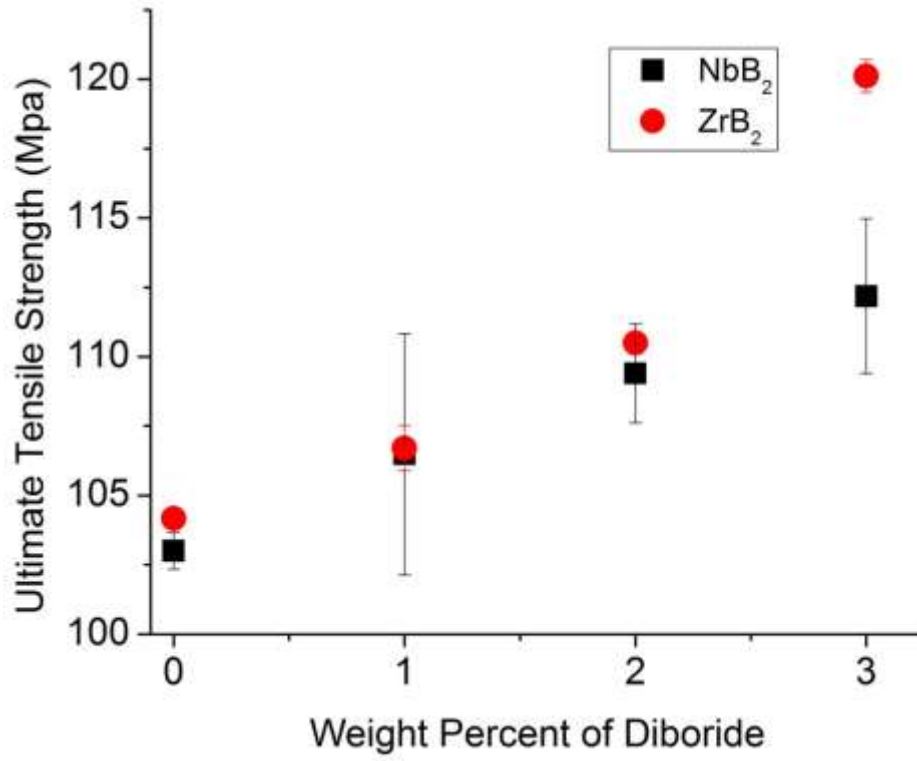


Figure 15 Measured tensile strength of aluminum wire samples

4. Experimental Procedure of Wire of Aluminum Treated with MgB₂ Nanoparticles

The same varioplanetary high energy ball mill described before was used for 5 h to reduce MgB₂ powder to nanoparticles. These nanoparticles were then mixed with pure aluminum pieces (~ 44µm) in the same ball mill in 4 intervals of 15 min divided by 5 min of rest to form diboride/Al pellets. To enhance the aluminum/diboride interface the 90%Al-10%MgB₂ pellet was sintered at 260°C for 30 minutes in a reduced vacuum atmosphere of about 4 kPa.

99.0% aluminum pellets were melted at 760°C and then the MgB₂/Al pellets were added into the molten aluminum. This molten material was poured into cylindrical graphite molds to produce ingots of 6 mm in diameter and varying amounts of MgB₂. The ingots with 0%, 0.5%, 1%, and 2%MgB₂ in weight were then cold-rolled to obtain wires with 4.7 mm diameter. Full annealing at 400°C for 5 hours permitted us to continue the cold rolling to reduce the wire diameter to 2.7 mm. Afterwards, we fully annealed the wires at 400°C for 5 h, so as to favor additional cold rolling to reduce the diameter to almost 1.4 mm. Another full annealing at 400°C for 5 h was used to reduce the diameter of the wire to 1 mm. All samples were characterized by x-ray diffraction, as described previously. The microstructures of the specimens were again observed using an optical microscope while the measurement of conductivity as % IACS was performed as indicated previously in Chapter 3.

4.1 Results

4.1.1 MgB₂ Nanoparticles

For this nanocomposite, we determined the most efficient milling procedure needed to produce the nanoparticles by testing different milling times from 1 hour to 5 hours. Figure 16 shows the x-ray diffraction patterns of the MgB₂ specimens during different stages of the milling process.

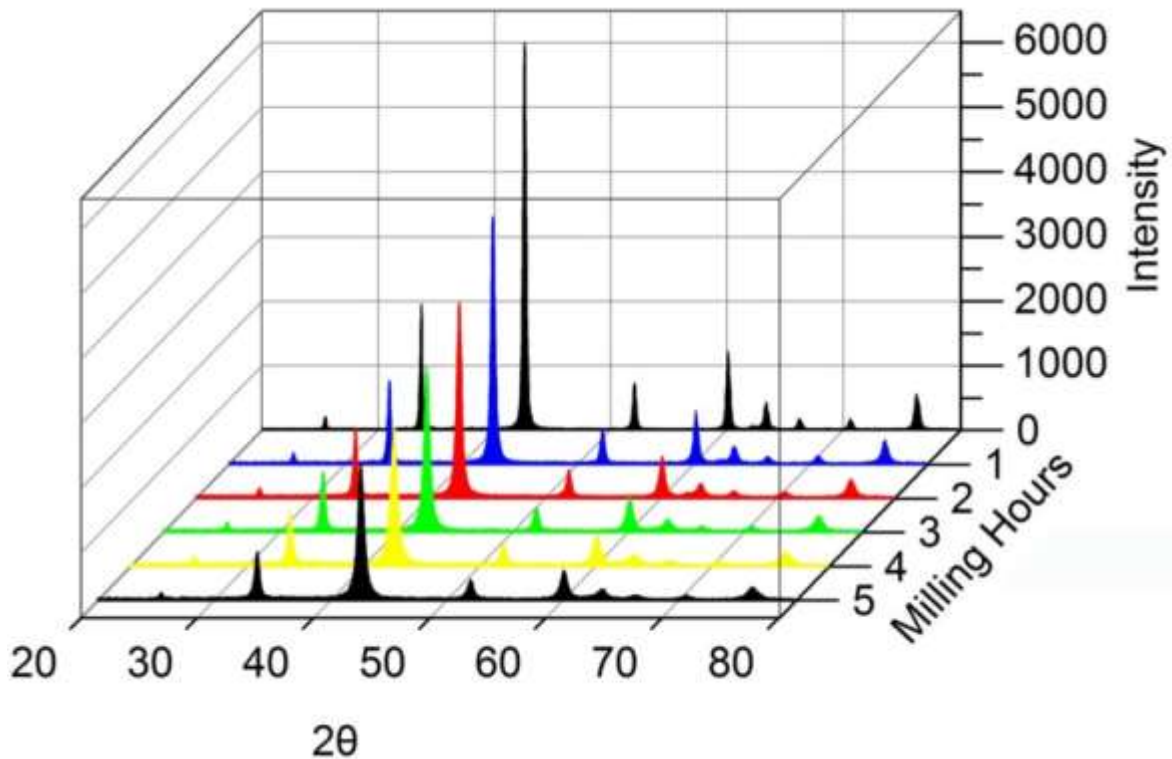


Figure 16 XRD pattern of MgB₂ specimen after 0 to 5 milling hours

Once again, the Scherrer equation permitted to estimate the average size of the ball milled diboride samples, based on the width of the largest peak. Subsequent millings at different times helped determine that after 5 hours the particle size is $\sim 17\text{nm}$, as shown in Figure 17.

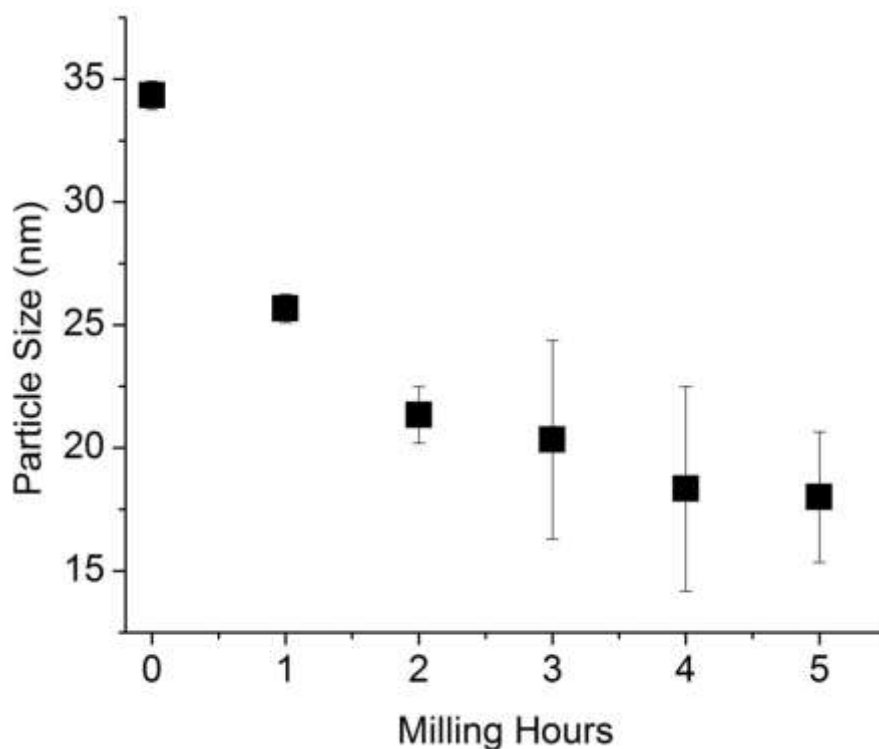


Figure 17 Computed mean MgB_2 particle size as a function of milling time

The scanning electron microscope images in Figure 18 show MgB_2 particles before the ball milling process and after 5 milling hours. The reduction in particle size of the diboride is evident. The MgB_2 particles obtained, which were milled for 5 h, had an approximate size of 17 nm, which was deemed appropriate to proceed with the planned experiments.

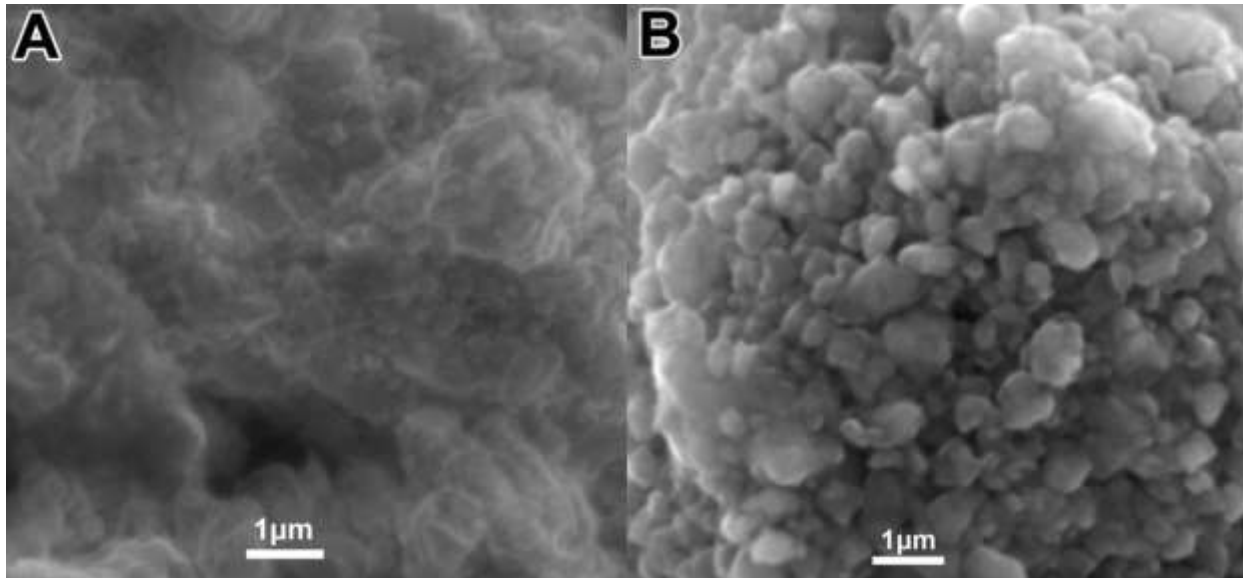


Figure 18 Secondary electron image of MgB_2 particles: (A) As-received MgB_2 , i.e. without ball milling; and (B) clusters of MgB_2 particles after 5 milling hours.

4.1.2 Nanocomposite Pellets

The nanosized diboride particles and 99.0% aluminum powder with an average size of $44 \mu\text{m}$ were mixed at 1000 rpm for one hour, in the same ball milling unit to form the diboride/Al pellets. As mentioned, all pellets were then sintered at 260°C in a reduced pressure atmosphere. Figure 19 shows the XRD patterns obtained from MgB_2/Al pellets. Any other additional unintended phases produced accidentally during the pellet fabrication were not detected.

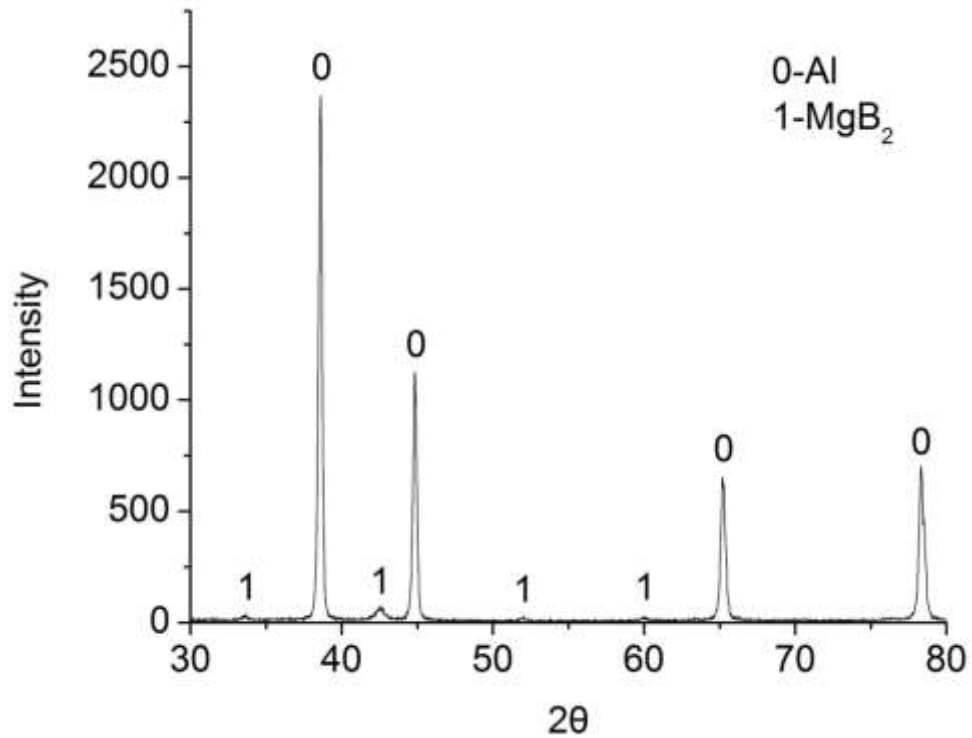


Figure 19 XRD pattern of MgB₂/Al composite pellet after sintering.

Figure 20 shows representative microstructures of the sintered pellets. The images allowed corroborating that MgB₂ particles are embedded in the Al matrix of the nanocomposite pellets.

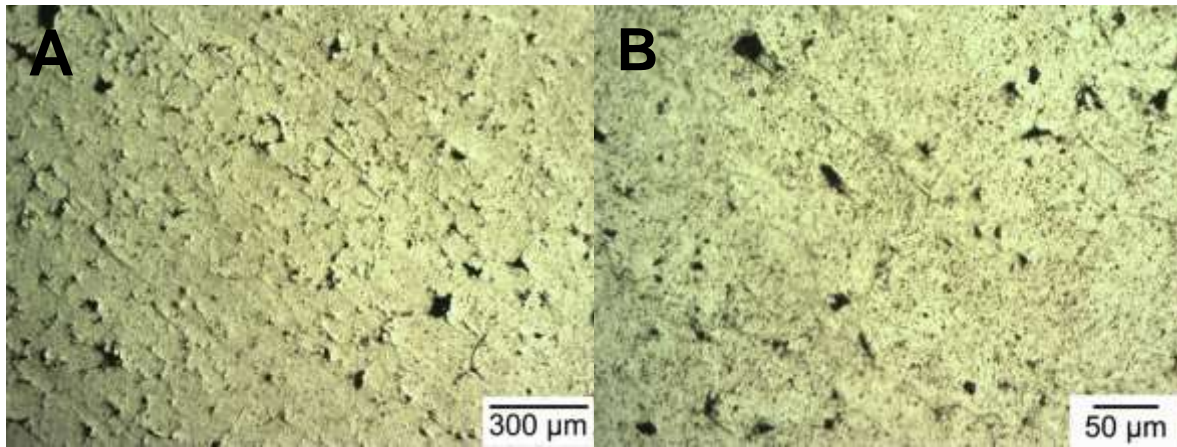


Figure 20 Optical micrographs of the nanocomposite pellets: (A) Al/MgB₂ pellet at low magnification; (B) Al/MgB₂ pellet at higher magnification.

4.1.3 Electrical Conductivity

The wires treated with MgB₂ 0% to 2% concentrations presented a conductivity from 62.7% to 48.97% IACS at 20°C, as shown in Figure 18. As expected, the conductivity decreases almost linearly with temperature.

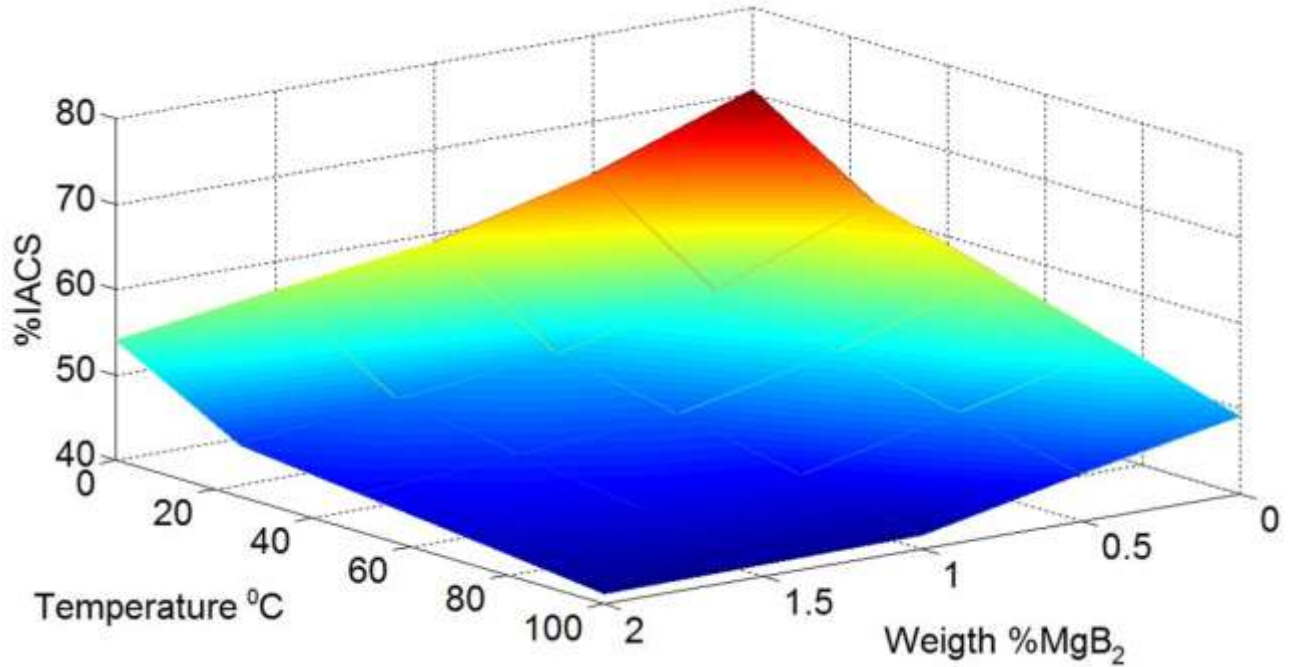


Figure 21 Effect of the MgB₂ nanoparticles and temperature on the electrical conductivity of aluminum wires (measured as percent of IACS).

4.1.4 Tensile Tests

As we can see, the ultimate tensile strength increases linearly, as the amount of diboride nanoparticles added, increased.

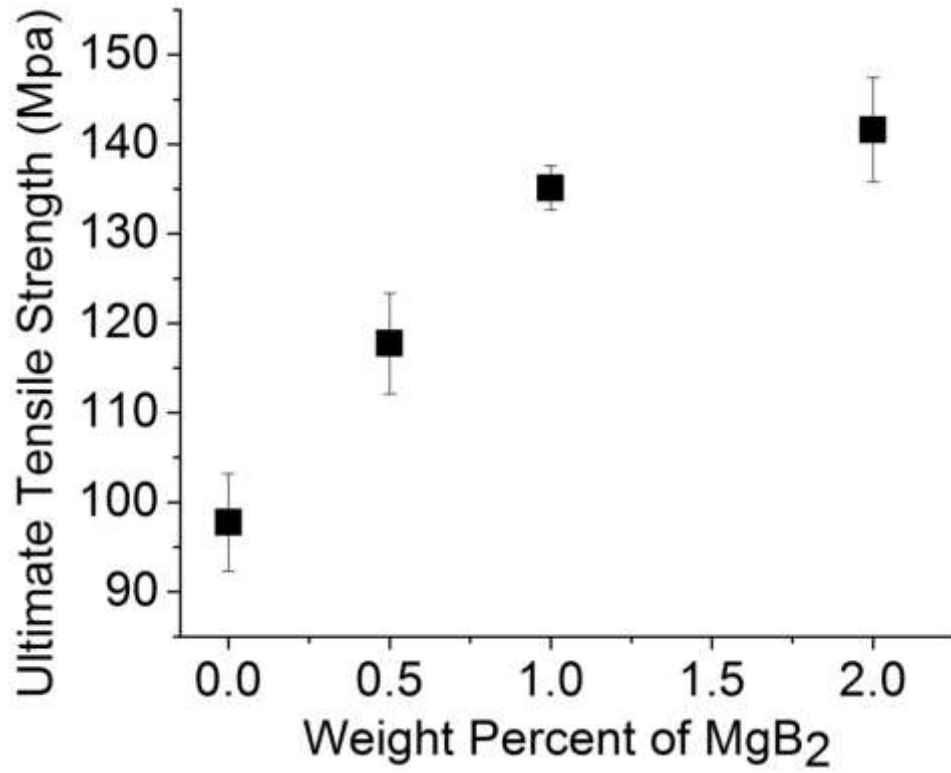


Figure 22 Measured ultimate tensile strength of aluminum wire samples

5. Discussion

To verify that the statistical significance of the addition of different nanoparticles on the electrical conductivity of the wires and the ultimate tensile strength, we carried out a multiple linear regression study. The nomenclature used in the equations is as follows: %IACS = Percent of International Annealed Copper Standard; T= temperature ($^{\circ}\text{C}$); %NbB₂ = weight percent of NbB₂; %ZrB₂ = weight percent of ZrB₂; %MgB₂ = weight percent of MgB₂ and UTS = Ultimate Tensile Strength (MPa).

Equations 1 to 3 are the resulting descriptive models of the electrical conductivity with respect to the temperature and amount of nanoparticles added . The values of the coefficients of multiple determinations, R^2 , for the fitted models, i.e. wires with NbB₂, ZrB₂, and MgB₂, are very high: 87.99%, 93.93% and 88.23% respectively. This indicates that the fitted linear models explain most of the variability of the response data. The resulting analysis of variance (ANOVA) (Table 1) further displays the fitting parameters and p-values for all models.

The Standard Error (SE) is the standard deviation of the distribution of the sample. This term also refers to an estimate of the standard deviation, derived from a particular sample.

$$\%IACS = 67.3481 - 1.0029 \cdot (\%NbB_2) - 0.1787 \cdot T \quad (1)$$

Equation is valid for ($3 < \%NbB_2 > 0$)

$$\%IACS = 68.5473 + 0.0432 \cdot (\%ZrB_2) - 0.1914 \cdot T \quad (2)$$

Equation is valid for ($Zr < \%ZrB_2 > 0$)

$$\%IACS = 62.9555 - 4.9441 \cdot (\%MgB_2) - 0.1522 \cdot T \quad (3)$$

Equation is valid for ($2 < \%MgB_2 > 0$)

For the model in Equation 1, i.e. wires treated with NbB₂, the p-value is just above 0.05, which indicates that increasing the addition of NbB₂/Al nanocomposite pellets barely affects the wire electrical conductivity. For Equation 2, the p-value calculated is significantly higher than 0.05, which implies that the addition of ZrB₂/Al nanocomposite pellets has no important effect on the wires' electrical conductivity. For Equation 3, the p-value calculated is 0.007, which indicates that increasing the amount of MgB₂/Al nanocomposite pellets affects the wire electrical conductivity. In summary, comparing the treated ZrB₂, NbB₂ and MgB₂ samples, electrical conductivity resulting from ZrB₂ treated wires were higher than for NbB₂ and MgB₂ treated wires.

Table 1 ANOVA of the model electrical conductivity of the wires

Parameter	%NbB ₂			%ZrB ₂			%MgB ₂		
	Value	SE Coefficient	p-value	Value	SE Coefficient	p-value	Value	SE Coefficient	p-value
Constant	67.348	1.200	0.000	68.547	0.956	0.000	62.955	1.871	0.000
Temperature	-0.178	0.014	0.000	-0.191	0.011	0.000	-0.1522	0.020	0.000
Diboride %	-1.003	0.555	0.085	0.043	0.424	0.920	-4.944	1.420	0.007

The ultimate tensile strength of the wires treated with nanoparticles increases with increasing nanoparticles content. Equations 5, 6, and 7 show the resulting descriptive model of the ultimate tensile strength with respect to the percentage of nanoparticles added.

$$\text{UTS} = 93.60 + 7.04 \cdot (\% \text{NbB}_2) \quad (4)$$

Equation is valid for ($3 < \% \text{NbB}_2 < 0$)

$$\text{UTS} = 96.40 + 8.11 \cdot (\% \text{ZrB}_2) \quad (5)$$

Equation is valid for ($3 < \% \text{ZrB}_2 < 0$)

$$\text{UTS} = 104.45 + 21.26 \cdot (\% \text{MgB}_2) \quad (6)$$

Equation is valid for ($2 < \% \text{MgB}_2 < 0$)

The R^2 values of the different models in equations 4, 5 and 6 are very high, 99.9%, 96.0%, and 81.8% respectively. This demonstrates that the calculated linear models are able to explain most of the variability observed in the response variable. The resulting ANOVA in Table 2 shows all fitted parameters and resulting p-values for the models.

Table 2 ANOVA of the model ultimate tensile strength

Parameter	%NbB ₂			%ZrB ₂			%MgB ₂		
	Value	SE Coefficient	p-value	Value	SE Coefficient	p-value	Value	SE Coefficient	p-value
Constant	93.60	0.309	0.000	96.40	1.650	0.000	104.450	4.687	0.000
Diboride	7.040	0.165	0.001	8.110	0.823	0.001	21.266	4.091	0.002

For both models, the SE of the fitted coefficients in equations 4, 5 and 6 are minimal. Particularly, the computed p-values are close to zero, which indicates that the diboride amounts are very effective in strengthening the wires, with MgB_2 bearing a larger effect. In summary, comparing the ZrB_2 , NbB_2 , and MgB_2 treated samples, tensile strength obtained for MgB_2 treated wires were higher than for MgB_2 and NbB_2 treated wires.

As observed in Figure 14 and Table 1, the electrical conductivity of the wires treated with the ZrB_2/Al nanocomposite remains mostly constant with a value over 63 IACS% at 20°C (close to pure aluminum) for all the additions. We attributed this result to the ZrB_2 low resistivity reported as $4.6 \mu\Omega\cdot\text{cm}$ [22]. Additionally, the conductivity was not significantly affected by severe plastic deformation, which is expected in most metals, according to Çetinarslan and Takata [23] [24]. As observed in Table 1, Figure 13, and Figure 21, the electrical conductivity of the wires treated with the NbB_2/Al and MgB_2/Al nanocomposites decreases significantly with the rising diboride content.

As already mentioned, in Figure 15 and Figure 22, one can see that the achieved tensile strengths of the aluminum wires turn out to be much higher than the strength normally reported for pure aluminum, i.e. 70MPa [21]. This behavior can be explained with strengthening theory. This theory does not state that with decreasing grain size, the mechanical strength increases. We can see this behavior in Figure 12, which shows micrographs which fully explain the increase in the tensile strength [25].

Table 1, Figure 15, and Figure 22 reveal that the tensile strengths of the wires have effectively increased as a function of the amount of NbB_2 , ZrB_2 and MgB_2 added. Magnesium diboride is the most effective in strengthening the wires. This particle strengthening has been extensively investigated, from an experimental and theoretical point of view. Existing models accounting for the dislocation motion and interaction are based on various descriptions of both particle geometry and the spatial distribution of particles [26]. When an isotropic and uniform distribution of nanoparticles is present in a given matrix, the composites are expected to be further Orowan-strengthened [27]. The Orowan mechanism is based on the principle that dislocations are obligated to surround or bow around the particles. As the stress increases, each dislocation meets itself, meaning that when it finds the dislocation segments, the particles and the dislocation segments equilibrate themselves. Shear stress applied to the solid and to the particles in particular should also be taken into consideration. In this case, the interaction between the dislocation and the particle increases the mechanical resistance because the energy that is required to “cut” the area of the gliding plane occupied by small particles also increases, resulting in a strengthening mechanism [25]. Similar trends are reported when using SiC , Al_2O_3 , Y_2O_3 , SiO_2 , and carbon nanotube particles by means of pure magnesium and various magnesium alloys as matrix material [27].

6. Conclusions

The experimental results of the present research allow several important conclusions to be stated:

- The methodology used allowed nanoparticles to be successfully added into molten Al to fabricate Al wires.
- NbB_2 , MgB_2 , and ZrB_2 nanoparticles were successfully produced and added into molten Al in the form of diboride/aluminum nanocomposite pellets to fabricate Al wires reinforced with diboride nanoparticles.
- Increasing levels of ZrB_2 had no significant effect on the aluminum wires electrical conductivity. On the other hand, NbB_2 and MgB_2 nanoparticles decreased the Al electrical conductivity. All results were substantiated via statistical analysis.
- Values of the longitudinal ultimate tensile strength of the wires were seen to increase as the obtained for higher levels of MgB_2 , NbB_2 , and ZrB_2 were elevated. Of these diborides, MgB_2 was the most effective in strengthening the wires.

7. References

- [1] K. Hanazaki, N. Shigeiri, and N. Tsuji, "Change in microstructures and mechanical properties during deep wire drawing of copper," *Mater. Sci. Eng. A*, vol. 527, no. 21–22, pp. 5699–5707, Aug. 2010.
- [2] S. Karabay, "Modification of AA-6201 alloy for manufacturing of high conductivity and extra high conductivity wires with property of high tensile stress after artificial aging heat treatment for all-aluminium alloy conductors," *Mater. Des.*, vol. 27, no. 10, pp. 821–832, Jan. 2006.
- [3] FAA and U. S. Federal Aviation Administration, *Airframe and Powerplant Mechanics*. pp. 5–1,5–5.
- [4] L. R. Russi, "Synthesis and Characterization of (AlMg) B 2 - Alumimun Based Composites and Nanocomposite," 2007.
- [5] T. T. Sasaki, R. a. Morris, G. B. Thompson, Y. Syarif, and D. Fox, "Formation of ultra-fine copper grains in copper-clad aluminum wire," *Scr. Mater.*, vol. 63, no. 5, pp. 488–491, Sep. 2010.
- [6] I. Sabirov, M. Y. Murashkin, and R. Z. Valiev, "Nanostructured aluminium alloys produced by severe plastic deformation: New horizons in development," *Mater. Sci. Eng. A*, vol. 560, pp. 1–24, Jan. 2013.

- [7] J. Tokutomi, K. Hanazaki, N. Tsuji, and J. Yanagimoto, "Change in mechanical properties of fine copper wire manufactured by continuous rotary draw bending process," *J. Mater. Process. Technol.*, vol. 212, no. 11, pp. 2505–2513, Nov. 2012.
- [8] J. Yanagimoto, J. Tokutomi, K. Hanazaki, and N. Tsuji, "Continuous bending-drawing process to manufacture the ultrafine copper wire with excellent electrical and mechanical properties," *CIRP Ann. - Manuf. Technol.*, vol. 60, no. 1, pp. 279–282, Jan. 2011.
- [9] H. Wang, D. Xing, X. Wang, and J. Sun, "Fabrication and Characterization of Melt-Extracted Co-Based Amorphous Wires," *Metall. Mater. Trans. A*, vol. 42, no. 4, pp. 1103–1108, Nov. 2010.
- [10] W. Tang and a. P. Reynolds, "Production of wire via friction extrusion of aluminum alloy machining chips," *J. Mater. Process. Technol.*, vol. 210, no. 15, pp. 2231–2237, Nov. 2010.
- [11] H. Ehsanian Mofrad, S. Raygan, B. Amin Forghani, K. Hanaei, and F. K. Ahadi, "Effect of cold-working and aging processes on the microstructure, mechanical properties and electrical conductivity of Cu–13.5%Mn–4%Ni–1.2%Ti alloy," *Mater. Des.*, vol. 41, pp. 182–191, Oct. 2012.
- [12] I. The and M. A. Mechanical, "Nomenclature 3.1," pp. 21–34.
- [13] M. Alloying, "Equipment for Mechanical Alloying 4.1," pp. 35–58.

- [14] L. Street, "8000M MIXER / MILL," no. 87011.
- [15] "Attritor, How attritor Works, Attritor working, Dry Grinding, Wet Grinding, Circulation Type Attritor, Ink Mixer, industrial attritors." [Online]. Available: http://www.attritor.in/attritor_working.html. [Accessed: 28-May-2013].
- [16] B. Harris, "Engineering Composite Materials," 1999.
- [17] O. M. Suárez, J. Vázquez, and L. Reyes-Russi, "Synthesis and Characterization of Mechanically Alloyed Al/AlxMg1-xB2 Composites," *Sci. Eng. Compos. Mater.*, vol. 16 [4], pp. 267–276, 2009.
- [18] C. B.D and S. S.R, *Elements of X-Ray Diffraction*, 3rd ed. New Jersey, 2001, pp. 167–184.
- [19] O. M. Suárez, D. S. Stone, and C. J. Kailhofer, "Measurement Of Electrical Resistivity in Metals and Alloys Using a Commercial Data Acquisition Software," *J. Mater. Educ.*, vol. volumen 20, pp. 341–356, 1999.
- [20] D. O. C. U. S. O. AMERICA, Ed., *National Bureau of Standards Copper wire tattles*, 3d Edition. WASHINGTON, 1914.
- [21] T. George E. and M. S. D., *Handbook of Aluminum*. New York: Physical Metallurgy and Processes, 2003, p. 67.
- [22] H. K. Inoshita, S. O. Tani, S. K. Amiyama, H. A. Mano, I. A. Kasaki, J. S. Uda, and H. M. Atsunami, "Express Letter Zirconium Diboride (0001) as an Electrically

- Conductive Lattice-Matched Substrate for Gallium Nitride Thermal expansion coefficient Temperature (C),” vol. 40, no. 12, pp. 1280–1282, 2001.
- [23] C. S. Çetinarslan, “Effect of cold plastic deformation on electrical conductivity of various materials,” *Mater. Des.*, vol. 30, no. 3, pp. 671–673, Mar. 2009.
- [24] N. Takata, S.-H. Lee, and N. Tsuji, “Ultrafine grained copper alloy sheets having both high strength and high electric conductivity,” *Mater. Lett.*, vol. 63, no. 21, pp. 1757–1760, Aug. 2009.
- [25] J. D. Verhoeven, *Fundamentos de Metalurgia Fisica*, Primera Ed. México, 1987, pp. 429–438.
- [26] S. Queyreau, G. Monnet, and B. Devincere, “Orowan strengthening and forest hardening superposition examined by dislocation dynamics simulations,” *Acta Mater.*, vol. 58, no. 17, pp. 5586–5595, Oct. 2010.
- [27] H. Dieringa, “Properties of magnesium alloys reinforced with nanoparticles and carbon nanotubes: a review,” *J. Mater. Sci.*, vol. 46, no. 2, pp. 289–306, Oct. 2010.
- [28] E. Purposes, M. Products, and C. Aluminum-, “Standard Specification for Aluminum 1350 – H19 Wire for Electrical Purposes 1,” pp. 1–4, 1975.
- [29] T. Covered and P. Properties, “Electrical and Chemical Properties – Supplier Data by Ceramaret Mechanical Properties at 20 ° C,” pp. 2–4, 2000.

- [30] E. Fereiduni and S. S. Ghasemi Banadkouki, "Reliability/unreliability of mixture rule in a low alloy ferrite–martensite dual phase steel," *J. Alloys Compd.*, vol. 577, pp. 351–359, Nov. 2013.

APPENDICES

APPENDIX A.

The purpose of conducting an additional experiment with Al-Al₂O₃ composites has been to study how the wire manufacturing process affected the material. The master alloy aluminum containing 2% wt alumina nanoparticles was provided by Prof. Xiaochun Li, currently at the University of California-Los Angeles.

A.1 Experimental Procedure of Aluminum Wire Treated with Alumina Nanoparticles.

Commercially pure aluminum pellets (99.5%) were melted at 760°C, inoculated with the master alloy and mechanically stirred. The treated aluminum melt was then poured into a cylindrical mold to produce 6 mm diameter ingots. These ingots were fully annealed at 400°C for 5 hours in order to cold-roll the ingot to fabricate wires with 2.6 mm diameter, i.e. a cross sectional area reduction of 81%. Full annealing at 400°C for 5 hours permitted to continue the cold rolling to reduce the wire diameter to 1.4 mm. Finally, another full annealing at 400°C for 5 hours facilitated more cold rolling to reduce the wire diameter to 1 mm.

The fractures of the specimens were observed with a scanning electron microscope JOEL JSM-6390. The microstructures of the specimens, i.e. the wires at different stages of the manufacturing process, were observed with an optical microscope. Standard tensile tests at room temperature were conducted using the low force universal testing machine mentioned before, following the standard ASTM B557 – 06 [22]. The measurement of the conductivity using % IACS was performed, as indicated in Chapter 3.

A.2. Results

A.2.1 Bending Properties

The ASTM B 230/B 230M – 07 standard used to test the wires recommends to one loop the wire around its own diameter with or without a mandrel [28]. This procedure is used to check if the wire possesses adequate plasticity to tolerate bends in a circuitry or transmission line. As Figure 23 (A through C) appears to demonstrate that aluminum wires treated with 0.25, 0.50, and 0.75 weight percent of Al_2O_3 particles do not bear such brittle fracture upon looping. For the aluminum wire treated with 1 wt.% Al_2O_3 particles, two fissures were visible (Figure 23 D).

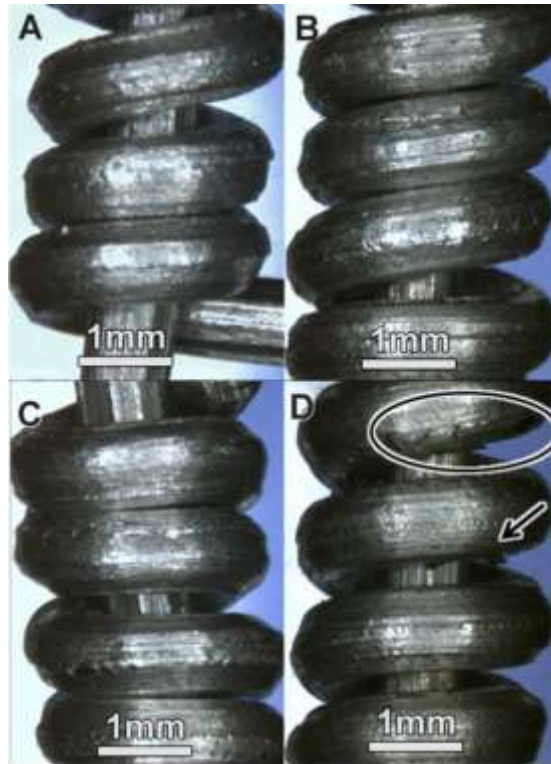


Figure 23 Bending (looping) test of aluminum wires treated with different weight percentage of Al_2O_3 nanoparticles: (A) 0.25(B) 0.5(C) 0.75(D) 1.0

A.2.2 Density of Wires

As one can see, in Figure 24, the wire density increased (no more than 1%) for larger amounts of alumina nanoparticles added. This may be due to the density of the alumina, which is 68% greater than the aluminum one.

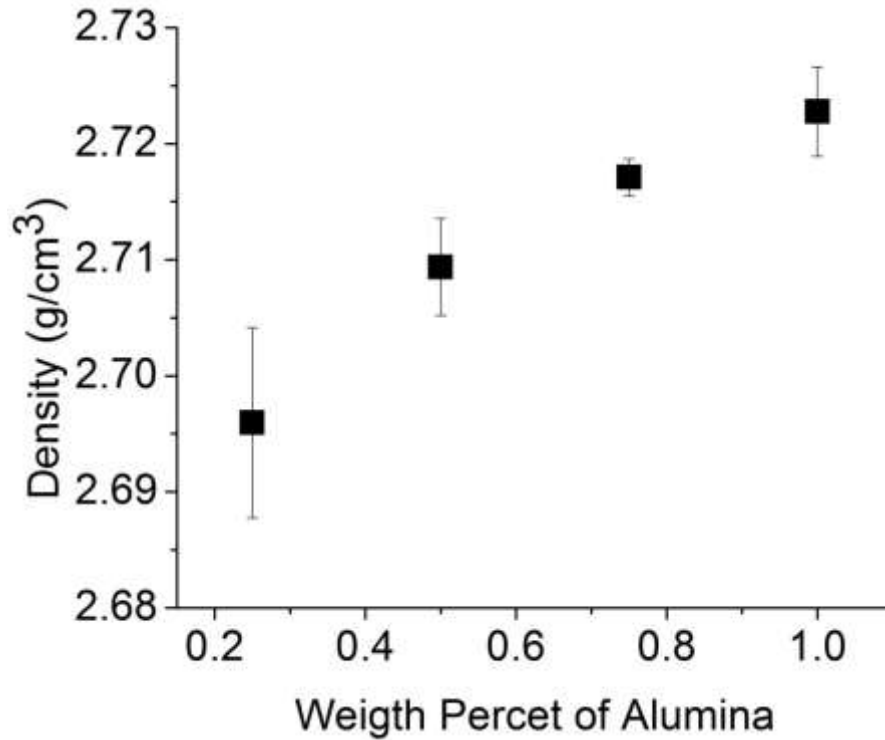


Figure 24 Measured density of aluminum wire samples as a function of the amount of alumina added.

A.2.3 Electrical Conductivity

The wires treated with alumina nanoparticles displayed lower electrical conductivity with respect to pure aluminum at 25°C, for alumina concentrations ranging from 0.25 % to 1 % in weight, as observed in Figure 25.

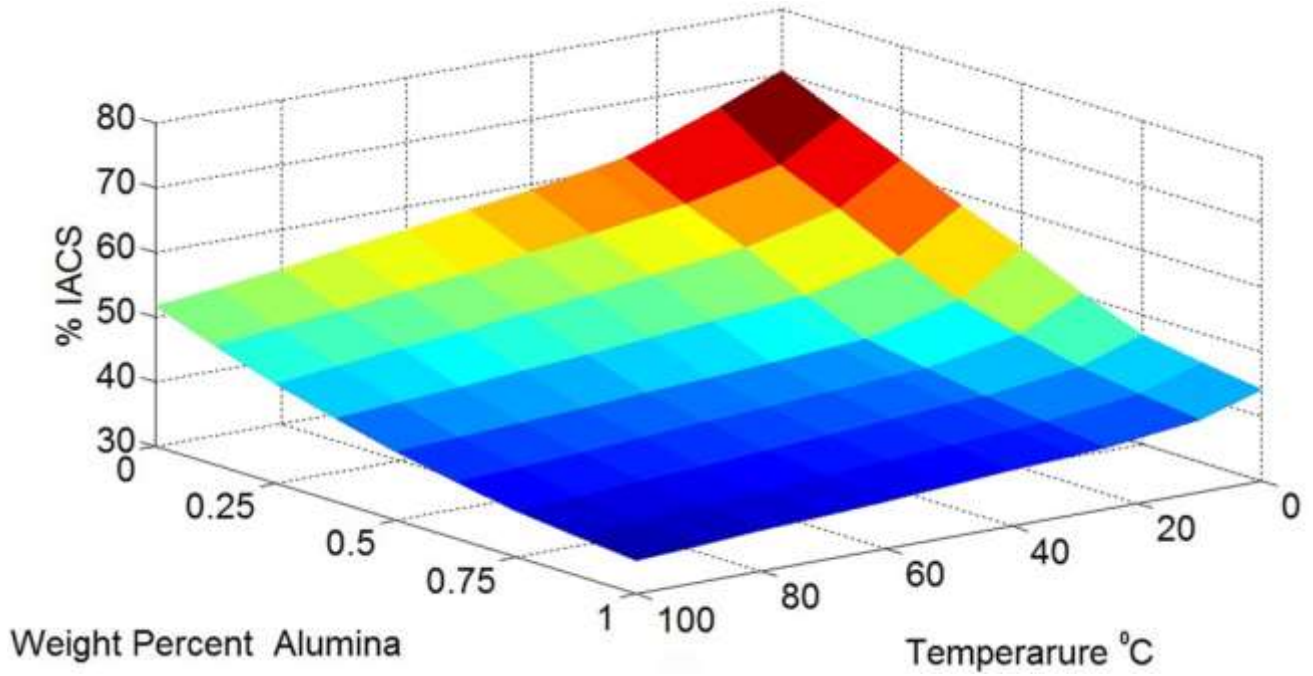


Figure 25 Effect of the amount of alumina nanoparticles added and temperature on the electrical conductivity of aluminum wires (measured as percent of IACS).

A.2.4 Tensile Test

As one can see in Figure 26 the ultimate tensile strength increases as the amount of alumina nanoparticles added increases.

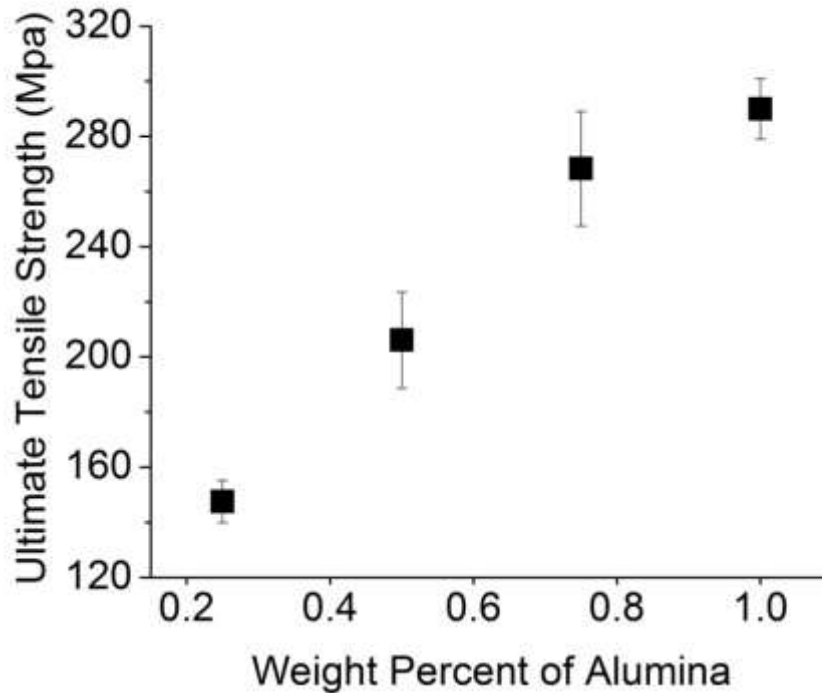


Figure 26 Average ultimate tensile strength of aluminum wire samples as a function of alumina added.

A.2.5 Macrograph of Wire Fracture

Figure 27 shows the aluminum wire fractures after the stress test was performed. ImageJ, an image analysis software, was used to determine the percentage of brittle and ductile fracture areas. Brittle area measurements (in percent) are shown in Figure 28 It is apparent that increasing the amount of alumina nanoparticles to be added result in raising the brittleness of the treated wires.

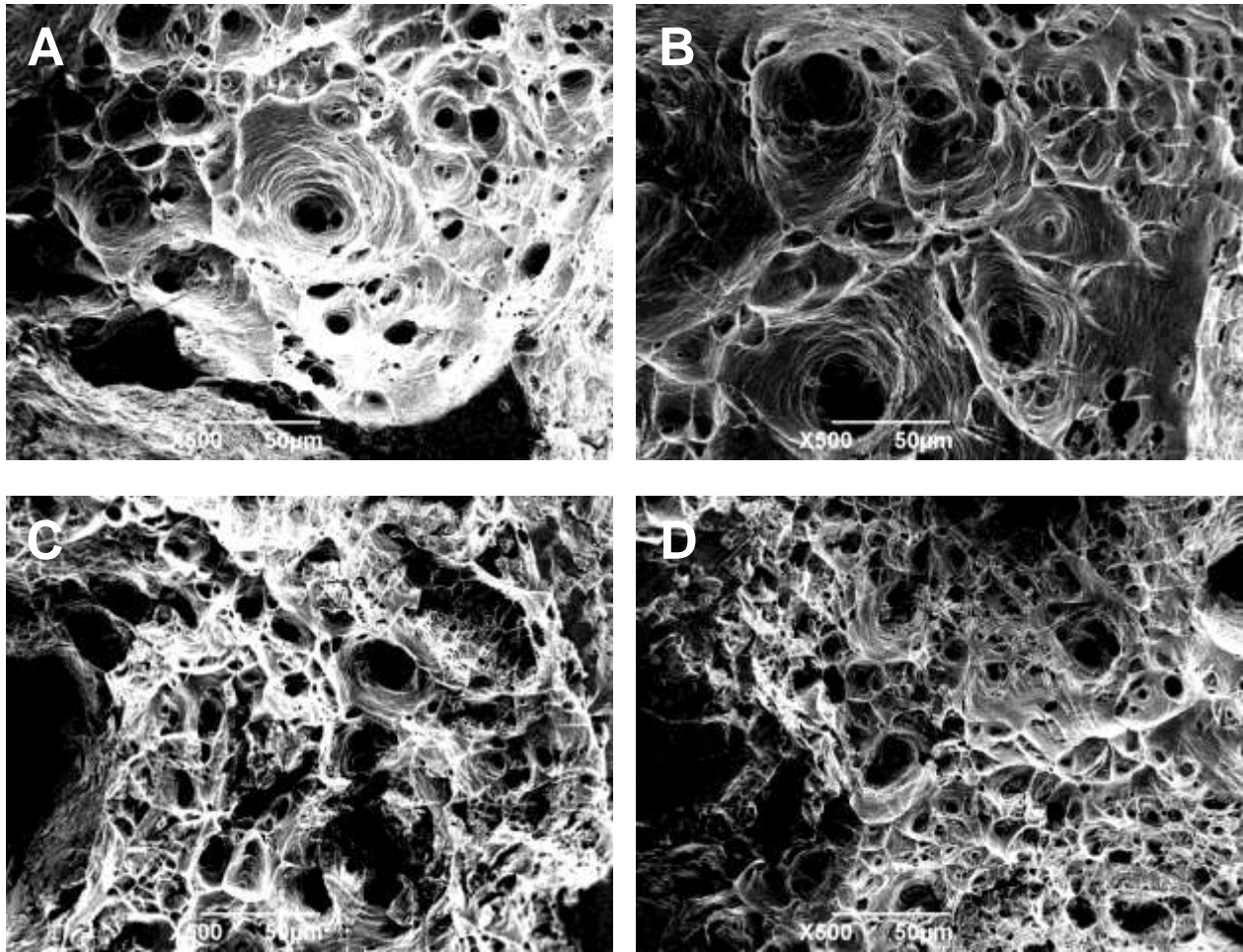


Figure 27. SEM images of tensile fracture surfaces of the aluminum wires treated with different weight percentage of Al₂O₃ nanoparticles: (A) 0.25 wt.%; (B) 0.5 wt.%; (C) 0.75 wt.%; and (D) 1.0 wt.%.

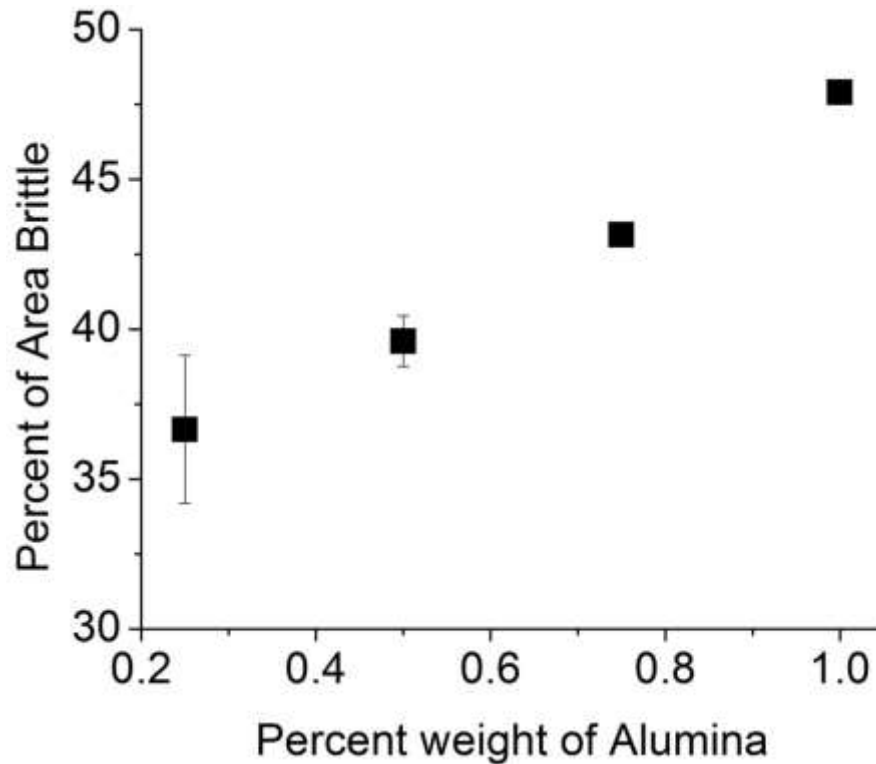


Figure 28 Percent of brittle fracture area of aluminum wire samples treated with alumina nanoparticles.

A.3 Discussion of Results

To study the statistical significance of the alumina addition effects on the electrical conductivity and ultimate tensile strength of the wires, we conducted a multiple linear regression analysis. Equations 7 and 8 show the resulting descriptive models of the electrical conductivity with respect to the temperature, the percentage of alumina added, and the ultimate tensile strength with respect to the percentage of alumina.

The R^2 values for both models, i.e. electrical conductivity and UTS, are high at 87.59% and 82.24%, respectively. The resulting analysis of variance (ANOVA) table (Table 3 and 4) further displays the fitting parameters and p-values for both models.

$$\%IACS = 61.8943 - 18.8141 \% \text{ Alumina} - 0.1117 \cdot T \quad (7)$$

$$UTS = 118.702 + 164.35 \% \text{ Alumina} \quad (8)$$

Equations are valid for ($1 < \% \text{ Al}_2\text{O}_3 < 0$)

Table 3 ANOVA of the model in Equation 7

Parameter	Value	SE Coefficient	p-Value
Constant	61.8922	2.3457	0.000
%Alumina	-18.8141	3.1807	0.000
Temperature	-0.1117	0.0209	0.000

Table 4 ANOVA of the model in Equation 8

Parameter	Value	SE Coefficient	p-Value
Constant	118.702	21.3507	0.001
%Alumina	164.350	31.1847	0.002

For the model in Equation 7, electrical conductivity with respect to the temperature and the percentage of alumina added, the p-value was 0.000, which indicates that increasing the amount of alumina decreases the conductivity of the wires. This can be explained because alumina possesses a high resistivity, which is estimated to exceed the $10^{14} \Omega \cdot \text{cm}$ at 20°C [29]. For the model in Equation 8, ultimate tensile strength of wires with respect to the percentage of alumina had a p-value of 0.002, which indicates that increasing the alumina content strengthens the wires.

As expected, the alumina content did affect the density of the wires, since the density of the alumina is 68.18% higher than aluminum. In analyzing the bending properties and the macrograph of wire fractures, increasing the alumina content of the samples caused loss of ductility. Using the mixture rule [30], equations 9 and 10 are obtained:

$$\text{ECM} = \text{EC}_{\text{Al}} \cdot V_{\text{Al}} + \text{EC}_{\text{Alumina}} \cdot V_{\text{Alumina}} \quad (9)$$

$$\text{UTSM} = \text{UTS}_{\text{Al}} \cdot V_{\text{Al}} + \text{UTS}_{\text{Alumina}} \cdot V_{\text{Alumina}} \quad (10)$$

ECM = Electrical conductivity of the mixture; EC_{Al} = Electrical conductivity of pure aluminum; $EC_{Alumina}$ = Electrical conductivity of alumina; UTSM = Ultimate tensile strength of the mixture; UTS_{Al} = Ultimate tensile strength of pure aluminum; $UTS_{Alumina}$ = Ultimate tensile strength of pure alumina; $V_{Alumina}$ = volume fraction of alumina nanoparticles and V_{Al} = volume fraction of pure aluminum.

The electrical resistivity at 20°C and tensile strength of aluminum were estimated to be $2.65 \cdot 10^{-8} \Omega \cdot m$ and 70 MPa, respectively [21]. The electrical resistivity at 20°C and compressive strength of aluminum is estimated to be $> 1 \cdot 10^{12} \Omega \cdot m$ and 1900-2000 MPa, respectively [29]. In the case of alumina, it was assumed that tensile strength equals compressive strength and that the electrical resistivity is $1 \cdot 10^{12} \Omega \cdot m$. In tables 5 and 6, one can observe the data obtained using the mixture rule and the experiments of the electrical conductivity and ultimate tensile strength with the percentage of error between experimental and modeled values.

Table 5 Electrical conductivity analysis using the mixture rule

Samples	ECM ($\text{S}\cdot\text{cm}^{-1}$)	ECM (IACS%)	Experimental ECM (IACS%)	%Error
Wires-0.25%Wt Al_2O_3	$3.77\cdot 10^5$	65.00	53.32	17.96
Wires-0.50%Wt Al_2O_3	$3.76\cdot 10^5$	64.84	44.77	30.95
Wires-0.75%Wt Al_2O_3	$3.75\cdot 10^5$	64.68	41.67	35.57
Wires-1.00%Wt Al_2O_3	$3.74\cdot 10^5$	64.52	39.55	38.70

Table 6 Ultimate tensile strength analysis using the mixture rule

Samples	UTSM (MPa)	Experimental UTSM (MPa)	%Error
Wires-0.25%Wt Al ₂ O ₃	127.3	147.53	-15.8
Wires-0.50%Wt Al ₂ O ₃	174.6	206.07	-18.0
Wires-0.75%Wt Al ₂ O ₃	221.9	268.32	-20.9
Wires-1.00%Wt Al ₂ O ₃	269.2	289.95	-7.7

The electrical conductivity values were lower than those estimated with the linear mixture rule. However, the ultimate tensile strength of the wires resulted in values higher than those estimated using the mixture rule.

As observed in Figure 25 and Table 3 that increasing percentage of alumina added and the temperature decreases the conductivity of the wires. for the case of the alumina This can be explained by alumina possessing a high resistivity, which is estimated to exceed the $>10^{14} \Omega \cdot \text{cm}$ at 20°C[8].

Table 4 and Figure 26 reveal that the tensile strengths of the wires have effectively increased as a function of the amount of Al_2O_3 . This particle strengthening has been extensively explained in the chapter 5.

A.4 Conclusions

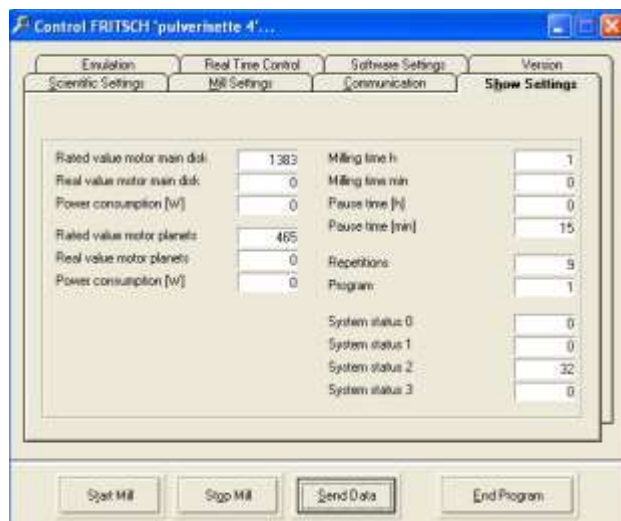
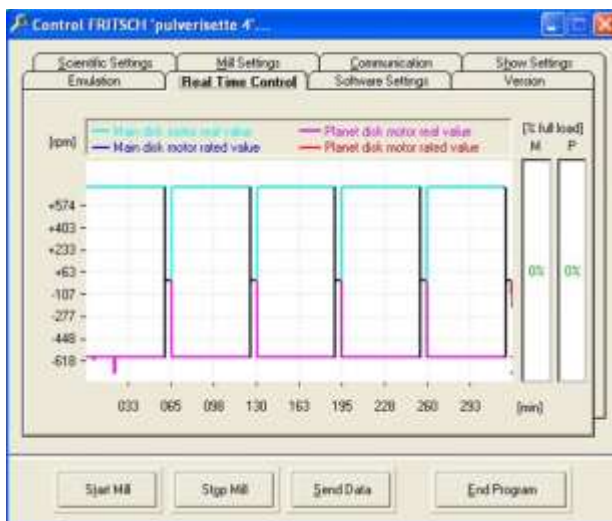
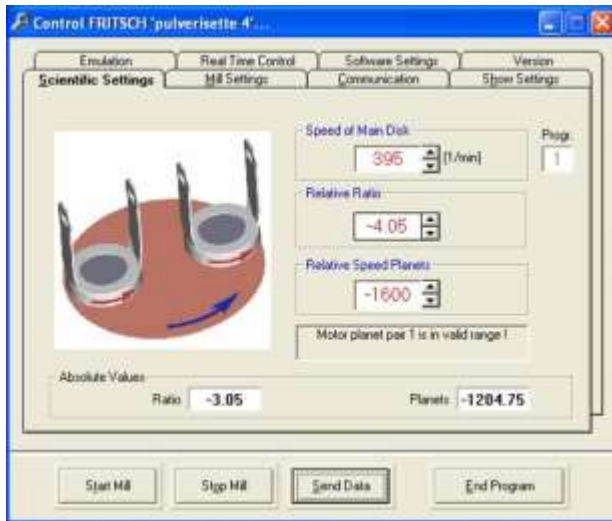
The experimental results of this thesis allowed stating several conclusions:

- The increasing levels Al_2O_3 nanoparticles decreased the electrical conductivity of those wires. The results were also corroborated via statistical analysis.
- Increasing values of the longitudinal ultimate tensile strength of the wires were observed a function of the amount Al_2O_3 of added.
- It is apparent that increasing the amount of alumina nanoparticles added results in raising the brittle area of the treated wires.

APPENDIX B. Vario-Planetary Ball Milling Pulverisette 4 Fritsch™

Software settings

B.1 Run setting for 10hr, 1600 rpm



B.1 Run setting for 1hr, 1000 rpm

